

The Pennsylvania State University  
The Graduate School  
Department of Aerospace Engineering

**NUMERICAL AND ANALYTICAL SOLUTIONS TO RAPID COLLISION  
AVOIDANCE MANEUVERS CONSTRAINED BY MISSION PERFORMANCE  
REQUIREMENTS**

A Thesis in  
Aerospace Engineering  
by  
Jason A. Reiter

© 2016 Jason A. Reiter

Submitted in Partial Fulfillment  
of the Requirements  
for the Degree of

Master of Science

May 2016

The thesis of Jason A. Reiter was reviewed and approved\* by the following:

David B. Spencer  
Professor of Aerospace Engineering  
Thesis Adviser

Karl M. Reichard  
Research Associate and Assistant Professor of Acoustics  
Head, Embedded Hardware/Software Systems and Applications Dept.

George A. Lesieutre  
Professor of Aerospace Engineering  
Head of the Department of Aerospace Engineering

\*Signatures are on file in the Graduate School

## **ABSTRACT**

Collision avoidance maneuvers to prevent orbital collisions between two catalogued objects are typically planned multiple days in advance. If the warning time is decreased to less than half-an-orbit in advance, the problem becomes more complex. Typically, the maneuver (assumed to be impulsive) would be placed at perigee or apogee and oriented in the direction that allows for a fuel-optimal maneuver to be performed well before the predicted collision. Instead, for rapid collision avoidance scenarios, finite burn propagation was applied to determine the thrust duration and direction required to reach a desired minimum collision probability. Determining the thrust time and direction for a wide range of orbits and spacecraft properties results in a semi-analytical solution to the collision avoidance problem anywhere in Low-Earth Orbit. The speed at which this method can be applied makes it valuable when minimal time is available to perform such a maneuver.

For many spacecraft missions, even the slightest change in the orbit of the spacecraft may significantly affect its ability to perform to its required specifications. With the high volume of debris in orbit, debris-creating events could occur with no advanced notice, making rapid collision avoidance scenarios a real possibility. Care must be taken to ensure that any potential collision is avoided while minimizing the effect of the maneuver on the spacecraft's mission performance. Assuming perfect knowledge of the states of all objects and that the possible collisions occur at high relative velocities, the required thrusting time to achieve a desired collision probability is found. Varying the

desired collision probability, the resulting changes in the required thrust duration time (and, thus, fuel use) can be observed, providing options for trading the fuel use and likelihood of a collision. Additionally, both of these variables contribute directly to the ability of the spacecraft to perform to the desired mission specifications. As the collision probability threshold and required burn time increase, the mission performance decreases. The level of robustness necessary in the mission specifications can be used to limit the desired collision probability threshold. This is accomplished by determining the time and fuel required to perform the collision avoidance maneuver to the desired probability level and analyzing the effect of the time spent away from the mission orbit and the quantity of fuel required to perform the maneuver on the mission performance. It was found that, for notification times less than around 20 minutes, it is best to decrease the collision probability as much as the available fuel will allow without regard for the time duration of the maneuver. As the notification time increases past 20 minutes, more emphasis can be placed on the time required to perform the entire maneuver and it was found that simultaneously minimizing the maneuver time and collision probability outweighed the slight extra fuel required for such a maneuver. Such analysis would prove significant in real-time spacecraft operations when determining an optimal collision probability threshold (typically a subjective variable) for rapid collision avoidance scenarios.

## TABLE OF CONTENTS

List of Figures.....	vii
List of Tables.....	viii
List of Symbols.....	ix
Acknowledgements .....	xi
Chapter 1. INTRODUCTION.....	1
1.1 Current Technology.....	4
1.2 Previous Research.....	6
Chapter 2. SPACECRAFT MANEUVERS.....	8
2.1 Orbital Elements and State Vectors.....	8
2.2 Types of Maneuvers.....	11
2.3 Orbital Regimes and Perturbations.....	17
Chapter 3. COLLISION AVOIDANCE.....	21
3.1 Covariance.....	21
3.2 Collision Probability and Separation Distance.....	23
Chapter 4. OPTIMIZING THE MANEUVER.....	27
4.1 Thrust Location.....	27
4.2 Coast Location.....	28
4.3 Thrust Direction.....	29
4.4 Numerical Method Optimization.....	31
4.5 Effect of Perturbations.....	35
Chapter 5. ANALYTICAL METHOD.....	36
Chapter 6. TRADE STUDIES.....	40
Chapter 7. TRADING A COMPLETE TRAJECTORY.....	44
7.1 Return Trajectories.....	44
7.2 Trade Study Metrics and Weights.....	46
Chapter 8. RESULTS.....	48
8.1 The Analytical Solution.....	48
8.2 Trade Study Comparisons.....	51

Chapter 9. CONCLUSIONS.....61  
References.....63

## LIST OF FIGURES

Figure 2.1 – The Six Classic Orbital Elements.....	9
Figure 2.2 – Lambert’s Problem Diagram.....	14
Figure 2.3 – N-Body Diagram.....	20
Figure 3.1 – Error Ellipsoids of Primary and Secondary Objects.....	22
Figure 4.1 – Left: RCN reference frame with respect to the Central-Body-Centered inertial reference frame (IJK). Right: $\alpha$ and $\beta$ thrust angles with respect to the RCN reference frame.....	24
Figure 4.2 – Separation Distance vs. Burn Duration for Impulsive and Finite Burn Maneuvers in Low-Earth Orbit.....	32
Figure 4.3 – Optimization Flow Chart to the Minimal Thrust Duration That Achieves the Desired Separation Distance.....	33
Figure 6.1 – Seven Step Trade Study Process.....	41
Figure 6.2 – Example Trade Study Decision Matrix.....	42
Figure 8.1 – Thrust Duration vs Separation Distance, Numerical and Analytical.....	50
Figure 8.2 – Thrust Duration vs Collision Probability, Numerical and Analytical.....	51

## LIST OF TABLES

Table 5.1 – Valid Range of Inputs for the Analytical Solution.....	38
Table 8.1 – Maneuver Options for 8-Minute Notification Time.....	53
Table 8.2 – Minimum Fuel Trade Studies for 8-Minute Notification Time, Equal Fuel and Time Weights.....	54
Table 8.3 – Minimum Fuel Trade Studies for 8-Minute Notification Time, Unequal Fuel and Time Weights.....	55
Table 8.4 – Minimum Fuel Trade Studies for 8-Minute Notification Time, Unequal Fuel and Time Weights, Decreased Probability Weight.....	55
Table 8.5 – Maneuver Options for 15-Minute Notification Time.....	56
Table 8.6 – Maneuver Options for 20-Minute Notification Time.....	57
Table 8.7 – Minimum Fuel Trade Studies for 20-Minute Notification Time, Equal Fuel and Time Weights.....	58
Table 8.8 – Minimum Fuel Trade Studies for 20-Minute Notification Time, Unequal Fuel and Time Weights.....	58
Table 8.9 – Maneuver Options for 30-Minute Notification Time.....	59
Table 8.10 – Minimum Fuel Trade Studies for 30-Minute Notification Time, Equal Fuel and Time Weights.....	60
Table 8.11 – Minimum Fuel Trade Studies for 30-Minute Notification Time, Unequal Fuel and Time Weights.....	60



## LIST OF SYMBOLS

$C$	Tesseral and Zonal Coefficient
$C_d$	Coefficient of Drag
$I_{sp}$	Specific Impulse [sec]
$P_{max}$	Maximum Probability
$R_E$	Radius of Earth [km]
$S$	Tesseral and Zonal Coefficient
$T$	Thrust [N]
$U$	Gravitational Potential [J/kg]
$a$	Semimajor Axis [km] / Acceleration [km/s <sup>2</sup> ]
$c$	Chord Distance [km]
$d$	Separation Distance [km]
$e$	Eccentricity
$g$	Acceleration Due to Gravity [m/s <sup>2</sup> ]
$m$	Mass [kg]
$r$	Position of the Primary Object [km]
$r_A$	Radius of Collision Cross-Sectional Integration [km]
$r_a$	Radius at Apogee [km]
$r_{ECI}$	Position in the Earth Centered Inertial Frame [km]
$r_{ECEF}$	Position in the Earth Centered Earth Fixed Frame [km]

$r_p$	Radius at Perigee [km]
$s$	Semiperimeter [km]
$t_{\text{burn}}$	Thrust Duration [sec]
$t_{\text{coll}}$	Time-to-Collision [sec]
$\mathbf{u}$	Velocity Unit Vector
$v_{\text{ECI}}$	Velocity in the Earth Centered Inertial Frame [km]
$v_{\text{CEEF}}$	Velocity in the Earth Centered Earth Fixed Frame [km]
$\alpha$	In-Plane Thrusting Angle [radians] / Lambert's Problem Angle [radians]
$\beta$	Out-of-Plane Thrusting Angle [radians] / Lambert's Problem Angle [radians]
$\delta$	Rotation Angle [radians]
$\mu$	Standard Gravitational Parameter [km <sup>3</sup> /s <sup>2</sup> ]
$\omega$	Rotation Rate of Earth [rad/s]
$\varphi$	Latitude [radians]
$\rho$	Atmospheric Density [kg/m <sup>3</sup> ] / Correlation Coefficient
$\sigma$	Standard Deviation [km]
$\sigma^*$	Companion Standard Deviation [km]
$\sigma_x$	Standard Deviation, X-Axis [km]
$\sigma_z$	Standard Deviation, Z-Axis [km]
$\theta$	True Anomaly [radians]

## ACKNOWLEDGEMENTS

I would like to first thank Dr. David Spencer for all of his help on this thesis and all of my research over these past two years. His wisdom and mentorship in my courses, research, and professional endeavors have proven to be invaluable time and time again. Dr. Karl Reichard and the Penn State Applied Research Lab merit thanks as well for providing me with a research assistantship to support my graduate education and my research on resilient control for centrifugal pump systems.

I would also like to thank one of my undergraduate professors at Cal Poly, Dr. Kira Abercromby, for inspiring me to pursue astrodynamics research through her numerous orbital mechanics courses and for continuing to support me past my undergraduate studies.

A special thanks goes to my family who have been encouraging me to pursue my dreams for as long as I can remember. My father, Adam, has been a constant source of inspiration by showing me what it means to put your all into your work through his own career. He has instilled in me so many important professional skills, such as public speaking, conversation skills, and networking. I wouldn't be who I am today without him. My mother, Dawn, showed me how to set standards for myself in everything that I do; higher than anyone else would expect of me. My sister, Amanda, has always been a major source of encouragement and someone I can look up to despite her lesser age. My

grandma, Elanor, my number one fan, is the person I look forward to sharing details of my achievements with the most. My grandpa, Harvard, is the reason that I became an engineer to begin with. His research in microbiology has inspired me to make the world a better place through my own work and keeps me going when the research seems endless. Together, they are the best support system I could ever ask for.

# Chapter 1

## Introduction

In typical debris collision avoidance scenarios (COLA), the optimal maneuver is first determined by analyzing the encounter region where the two objects are predicted to collide. In situations where both the primary and secondary bodies can be tracked, their positions and velocities are determined to within their associated errors in the corresponding position covariance ellipsoids. Though not necessary for most cases with near-circular orbits, the covariance ellipsoids may be oriented for which the velocities are not perfectly aligned with their major principal axes. At the predicted time of collision, the covariance data is used to determine a maximum probability of collision and miss distance for the encounter. For any collision avoidance scenario, the goal is to reach a desired separation distance between the two objects at the predicted time of collision by performing a fuel-optimal maneuver.<sup>1,2</sup>

One main factor driving the planning of the maneuver is the starting and desired orientation of the primary object. Depending on the current operating conditions, the spacecraft may be pointed in a certain direction to best utilize its solar panels, scientific equipment, or other directional hardware. Time must be allotted to re-orient the spacecraft so that the main thrusters are pointed in the desired direction to perform the maneuver. Additional time will be allotted to ensure that the thrust is applied at apogee or

perigee, the most efficient locations in orbit to change the energy of the object. With these in mind, a maneuver is planned (assuming an impulsive burn) to reach the desired separation distance at the predicted time of collision with the least amount of fuel. These maneuvers can take hours, if not days, to plan and optimize.<sup>3</sup>

Unfortunately, with the uncertainty in the position of any two objects and the inability to track objects smaller than 10 cm in diameter, not all collisions can be avoided.<sup>4</sup> Debris from such a collision or other debris-creating events could put other satellites on collision courses with the newly-created debris with minimal time until the collision (possibly even less than half-an-orbit in duration). Currently, minimal previous work exists in avoiding collisions with such a small notification time.

When planning avoidance maneuvers for collisions between two catalogued objects, covariance data is often known for both objects. However, when the secondary object is newly-created, less opportunity exists to determine similar characteristics. Therefore, in scenarios with minimal time-to-collision, the secondary object must be considered as only a point mass and the probability must be determined with the information known about the primary object (its covariance assumed to be oriented in the direction of the velocity vector). In addition, it is assumed that no time is available to rotate the spacecraft to a more desirable orientation, so the thrust is assumed to be applied in the original orientation, and the thrust magnitude must be chosen as such.<sup>4</sup>

Collision avoidance maneuvers with less than half-an-orbit to both plan and execute involve additional complexities not found in typical advanced notification avoidance maneuvers due to the limited time available. For instance, finite burn analysis must be applied instead of assuming an impulsive burn maneuver. The limited time

available also leads to complexity in choosing both an optimal burn direction and burn location, which will both be covered in detail later. Working under these assumptions, a numerical solution can be determined for a fuel-optimal avoidance maneuver.

It is the analysis of the optimal burn direction, however, that led to the discovery of a semi-analytical solution to the problem. Assuming that the spacecraft of interest is in Low-Earth Orbit (LEO), a semi-analytical solution to the fuel-optimal collision avoidance maneuver is solved. This is accomplished by minimizing the finite burn time to reach the minimum separation distance at the time of closest approach for a given spacecraft location, thrust magnitude (assumed to be constant), thrust direction, and remaining time until the collision (time-to-collision). Once a relationship between the optimal burn time and the desired separation distance at the time of closest approach is found, the separation distance can be converted into a desired collision probability threshold, resulting in a single relationship between the spacecraft parameters, the required burn time, and the desired collision probability threshold.

Varying the desired collision probability, the resulting changes in the required thrust duration time (and, thus, fuel use) can be observed, providing options for trading the fuel use and likelihood of a collision. Additionally, both the probability of collision and the fuel use contribute directly to the ability of the spacecraft to adhere to the desired mission specifications. As the maximum collision probability and required burn time increase, the mission performance decreases with it. The level of robustness necessary in the mission specifications can then be used to limit the desired maximum collision probability. This is accomplished by determining the time and fuel required to perform the collision avoidance maneuver to the desired probability level and analyzing the effect

of the time spent away from the mission orbit and the quantity of fuel required to perform the maneuver on the mission performance. It was found that, for notification times less than around 20 minutes, it is best to decrease the collision probability as much as the available fuel will allow without regard for the time duration of the maneuver. As the notification time increases past 20 minutes, more emphasis can be placed on the time required to perform the entire maneuver and it was found that simultaneously minimizing the maneuver time and collision probability outweighed the slight extra fuel required for such a maneuver. These observations allow us to determine an optimal maximum collision probability (typically a subjective variable) for rapid collision scenarios.

### **1.1 Current Technology**

Each entity involved in the operations of spacecraft, whether government, private, or an FFRDC (Federally Funded Research and Development Center), has its own software for spacecraft collision avoidance. At The Aerospace Corporation<sup>5</sup>, in their support of U.S. National Security Space Systems, the decision to perform a collision avoidance maneuver is based on a cost–risk analysis that requires a quantifiable measure of risk. Unlike a keep-out criterion, collision probability provides the needed quantification of risk. The collision probability is weighed against the propellant consumed and shortened operational life span of the spacecraft and the value of the asset can be used to establish a collision risk threshold. In order to perform maneuvers as efficiently as possible, a four-dimensional space is searched for the optimal solution including the time of application, velocity magnitude, and direction (right ascension and declination) of the applied maneuver. Computational efficiencies in propagation,



collision probability calculation, and optimization are required to allow sufficient time for maneuver planning. This method, in which the collision probability prediction was made more efficient by replacing a two-dimensional integral with a one-dimensional path integral (increasing computational speed by a factor of 20), was applied to determine an actual maneuver for a geostationary asset while taking into account multiple possible conjunctions and was found to have worked as planned at reducing the collision probability.<sup>5</sup>

Given the on-going necessity for collision avoidance maneuvers, similar tools have also been developed for use in concurrence with Analytical Graphics Inc.'s STK (Satellite Tool Kit).<sup>6</sup> AGI themselves developed such a tool that can perform parametric studies of single-axis and dual-axes maneuvers by assessing changes in the combined object's cross-sectional surface-area in the encounter plane and exploring candidate times and the required change in velocity ( $\Delta V$ ) for possible avoidance maneuvers. For the determined time of closest approach, the tool reads the positions, velocities, covariances and physical sizes of both objects from STK. Then, given an upper bound on  $\Delta V$  and a range of allowable maneuver times, the tool maps out collision probability contours.<sup>6</sup> Despite the growing availability of such tools, none are currently being employed within the industry that can solve for optimal rapid collision avoidance maneuvers in the allotted time.

## 1.2 Previous Research

While previous research has been performed in solving rapid collision avoidance maneuvers and in determining analytical solutions for more thoroughly planned maneuvers, none has yet to be published combining the two. One publication, reference [7], discusses a new approach to finding the optimal collision avoidance maneuver considering multiple possible conjunctions within a short time period by applying a genetic algorithm. The paper demonstrates a handful of test cases of varying complexities and appears to be a valid alternative to the analytical solution approach. Like the research by Patera and Peterson<sup>5</sup> mentioned above, the solution considers multiple possible conjunctions and aims to decrease computation time but, in this case, has yet to be verified.

Research has also been performed at the Technical University of Madrid in formulating collision avoidance maneuvers as an eigenvalue problem.<sup>8</sup> In doing so, the authors created an analytical solution to minimize the maneuver cost while maximizing the separation distance. The optimization is based on a linear relation between the b-plane impact point displacement and the applied maneuver impulse.<sup>9</sup> However, this research is operating under the assumption that the applied burn is impulsive. As is demonstrated in Chapter 5, though, the burn cannot be assumed to be impulsive for rapid response maneuvers. Though this may be a high accuracy analytical solution, it unfortunately cannot be applied to the research presented in this paper where finite burn analysis is used instead.

A second paper [10] detailing an analytical collision avoidance maneuver solution formulated as a typical optimal feedback control problem with a penalty term

incorporated into the performance index, and designed such that the penalty increases sharply as two objects approach each other. A two-point boundary value problem was formed for a standard Hamiltonian system, resulting in a near-optimal control law represented as a truncated power series in feedback form. This algorithm was able to generate near-optimal trajectories without any initial guess or iterative process. Though this is an analytical solution and can be solved with minimal computational resources, its applications to the research presented in this paper are minimal given that the optimal control problem is unnecessary when a single optimal thrusting angle can be assumed for rapid response maneuvers.

A final publication was found related to the research presented here in which a method for reactive collision avoidance (RCA) is presented, which plans acceleration-limited trajectories in real-time to avoid the incoming spacecraft.<sup>11</sup> The feasibility of RCA-based formation path-planning was established by showing that the cost penalty of reactive as compared to predictive collision avoidance is on the order of 50% and that collisions in collision-unconstrained formation maneuvers are very rare. They demonstrated that, by accepting a probabilistically minor amount of sub-optimality, scalable formation path-planning is possible. Then, the paper continued on to present a three-dimensional, fuel-optimal RCA algorithm. Rather than finding the globally optimal avoidance trajectory, it was shown that a greedy RCA algorithm was both fast and effective. Though not applicable in this scope of this paper, this application of RCA may be useful in the future when looking to apply the research presented in this paper to real-time rapid response collision avoidance maneuvers.

## Chapter 2

### Spacecraft Maneuvers

When determining the fuel required to avoid an object in-orbit, an analysis of the avoidance maneuver is required. To calculate the maneuver, the position and velocity of the spacecraft is described using either orbital elements or state vectors. With the state known, the desired type of maneuver is chosen based on the time available, the fuel allocated for the maneuver, and the starting and desired location of the spacecraft. These maneuvers do vary, however, based on the orbital regime that the collision is predicted to occur in, which determines the perturbing forces acting on the spacecraft. This chapter explains in detail the maneuvers considered in this collision avoidance research.

#### 2.1 Orbital Elements and State Vectors

Six constants and time are required to completely describe the orbit of a satellite in orbit about the Earth. For most propagation methods, the six components of the state vectors  $\mathbf{r}$  and  $\mathbf{v}$  are sufficient. To fully understand the shape of the orbit, however, the classic orbital elements must be determined. To describe the size and shape of the orbit, the semimajor axis,  $a$ , and eccentricity,  $e$ , are used. The next three constants are used to describe the orientation of the orbit plane. The first, inclination ( $i$ ), is defined as the angle between the orbit plane and the equatorial plane. The right ascension of the ascending

node, or RAAN, is represented by  $\Omega$  and is defined as the angle between the line connecting the center of the Earth to the first point of Aries and the location of the ascending node (where the satellite crosses the equatorial plane). The argument of perigee,  $\omega$ , is the angle between the same node and perigee (the point of the orbit closest to the earth). This leaves one last orbital element, the true anomaly ( $\theta$ ), which defines the location of the satellite in the orbit with respect to perigee. These six elements, visualized in Fig. 2.1, completely describe the position and velocity of the satellite in its orbit. Throughout this paper, these elements will be used to describe all orbits considered.<sup>12</sup>

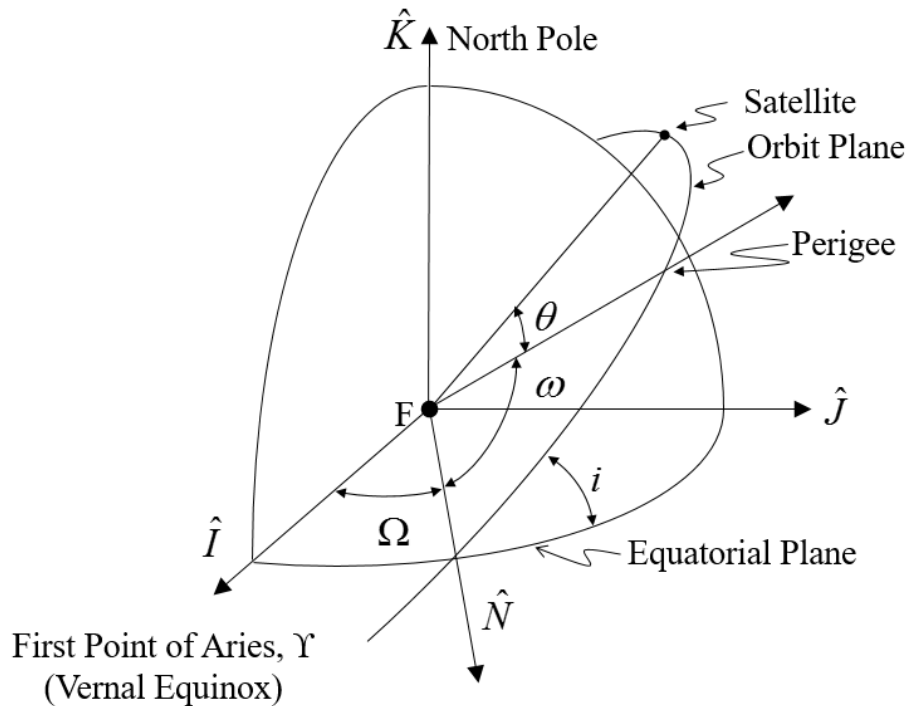


**Figure 2.1. The Six Classic Orbital Elements.**

Though the orbital elements are the easiest to visualize, propagating the orbit using them is less accurate than with the position and velocity state vectors. Fortunately, it is possible to transform from the orbit element set to the state vectors. First, the angular momentum,  $h$ , is

$$h = \sqrt{\mu a(1 - e^2)} \quad (2.1)$$

where  $\mu$  is the standard gravitational parameter of the Earth. Now, the position and velocity in the Earth Centered Inertial Frame (ECI) can be found from

$$\mathbf{r}_{ECI} = \frac{h^2}{\mu} \frac{1}{1 + e \cos \theta} \begin{bmatrix} \cos(\theta) \\ \sin(\theta) \\ 0 \end{bmatrix} \quad (2.2)$$

and

$$\mathbf{v}_{ECI} = \frac{\mu}{h} \begin{bmatrix} -\sin(\theta) \\ e + \cos(\theta) \\ 0 \end{bmatrix} \quad (2.3)$$

To transfer from the ECI frame to the Earth Centered Earth Fixed (ECEF) frame, a direction cosine matrix must be used:

$$Q = \begin{bmatrix} -\sin(\Omega) \cos(i) \sin(\omega) + \cos(\Omega) \cos(\omega) & \cos(\Omega) \cos(i) \sin(\omega) + \sin(\Omega) \cos(\omega) & \sin(i) \sin(\omega) \\ -\sin(\Omega) \cos(i) \cos(\omega) - \cos(\Omega) \sin(\omega) & \cos(\Omega) \cos(i) \cos(\omega) - \sin(\Omega) \sin(\omega) & \sin(i) \cos(\omega) \\ \sin(\Omega) \sin(i) & -\cos(\Omega) \sin(i) & \cos(i) \end{bmatrix} \quad (2.4)$$

Then, the transformation becomes

$$\begin{bmatrix} \mathbf{r}_{ECEF} \\ \mathbf{v}_{ECEF} \end{bmatrix} = Q' \begin{bmatrix} \mathbf{r}_{ECI} \\ \mathbf{v}_{ECI} \end{bmatrix} \quad (2.5)$$

where  $'$  denotes the transpose of  $Q$ . With the state vectors now known, the spacecraft's position and velocity can be found at any point in time by propagating the spacecraft's

location forward using MATLAB's ordinary differential equation solver, ode45 (a fourth and fifth order Runge Kutta solver with variable time steps).

The propagator, ode45, is based on the Dormand-Prince method and provides fourth-order accuracy with a fifth order error control, and propagates the orbit forward in time by integrating the equations of motion. In orbit, the acceleration of an object is defined as<sup>13</sup>

$$\mathbf{a} = -\frac{\mu}{\|\mathbf{r}\|^3} \begin{bmatrix} r_x \\ r_y \\ r_z \end{bmatrix} \quad (2.6)$$

At each time step, MATLAB numerically integrates the inputted velocity vector values and the calculated acceleration values to determine updated position and velocity state vectors at the new location. The position and velocity of the spacecraft at the notification time determines the location and type of maneuver necessary to successfully avoid the debris.

## 2.2 Types of Maneuvers

Maneuvers can be broken down into two types: impulsive and finite burn. When the time available to perform the maneuver is significantly greater than the required burn duration, the burn can be assumed to be impulsive. In this research, two types of impulsive burn maneuvers, the minimum-fuel Hohmann transfer and the minimum-time Lambert's problem, were considered.

The Hohmann transfer minimizes fuel by performing only two burns at the most effective locations to do so. Departing the original orbit, the first burn is placed at perigee

and the second burn is placed (in the reverse direction) at apogee of the final orbit upon arrival. The total  $\Delta V$  (change in velocity) for this maneuver is calculated by summing the difference between the orbital velocity of the original orbit and the orbital velocity of the transfer arc at the departure point and the difference between the orbital velocity of the final orbit and the orbital velocity of the transfer arc at the arrival point. A Hohmann transfer involves solving for the three different angular momenta: the original orbit, the transfer orbit, and the final orbit. These are expressed as

$$h_1 = \sqrt{2\mu} \sqrt{\frac{r_{p1} \cdot r_{a1}}{\|r_{p1} + r_{a1}\|}} \quad (2.7)$$

$$h_2 = \sqrt{2\mu} \sqrt{\frac{r_{p1} \cdot r_{a2}}{\|r_{p1} + r_{a2}\|}} \quad (2.8)$$

$$h_3 = \sqrt{2\mu} \sqrt{\frac{r_{p2} \cdot r_{a2}}{\|r_{p2} + r_{a2}\|}} \quad (2.9)$$

where  $r_p$  and  $r_a$  are the perigee and apogee of the orbits, respectively, 1 denotes the original orbit, and 2 denotes the transfer orbit.<sup>13</sup> The orbital velocity at each departure/arrival point for each of the three orbits can then be found simply from

$$v = h/r \quad (2.10)$$

This gives four different velocity values: departure from the original orbit, arrival on the transfer orbit, departure from the transfer orbit, and arrival on the final orbit. The total velocity change required is then found to be

$$\Delta V = |v_{p2} - v_{p1}| + |v_{a3} - v_{a2}| \quad (2.11)$$



where  $p$  denotes the departure point,  $a$  denotes the arrival point,  $1$  denotes the original orbit,  $2$  denotes the transfer orbit, and  $3$  denotes the final orbit. Substituting in the velocity values and the angular momenta values gives

$$\Delta V = \left| \sqrt{\frac{\mu}{r_i}} - \sqrt{2\mu \left( \frac{1}{r_i} + \frac{1}{r_i+r_f} \right)} \right| + \left| \sqrt{2\mu \left( \frac{1}{r_f} + \frac{1}{r_i+r_f} \right)} - \sqrt{\frac{\mu}{r_f}} \right| \quad (2.12)$$

The time to perform this maneuver is equal to the period of the transfer orbit divided by two:<sup>5</sup>

$$\Delta t = \frac{\pi}{\sqrt{\mu}} a^{3/2} \quad (2.13)$$

where  $a$  is the semimajor axis of the transfer orbit.

The minimum-time solution is solved using Lambert's problem, the transfer of a spacecraft from one point in space to another. With the starting and ending locations (any location in the orbit) specified, Lambert's problem can be used to determine the range of transfer times available to perform the maneuver, as well as the corresponding semimajor axis value of the transfer arc. When desired, the minimum-time solution can be found.

Starting with the two locations, the angle between them is found using<sup>7</sup>

$$\Delta\theta = \tan^{-1} \left( \frac{\|\mathbf{r}_i \times \mathbf{r}_f\|}{\mathbf{r}_i \cdot \mathbf{r}_f} \right) \quad (2.14)$$

Now the chord between the two points,  $c$ , can be found using the law of cosines

$$c = \sqrt{\|\mathbf{r}_i\|^2 + \|\mathbf{r}_f\|^2 - 2\|\mathbf{r}_i\|\|\mathbf{r}_f\|\cos(\Delta v)} \quad (2.15)$$

where  $c$  and  $v$  are defined in Fig. 2.2.

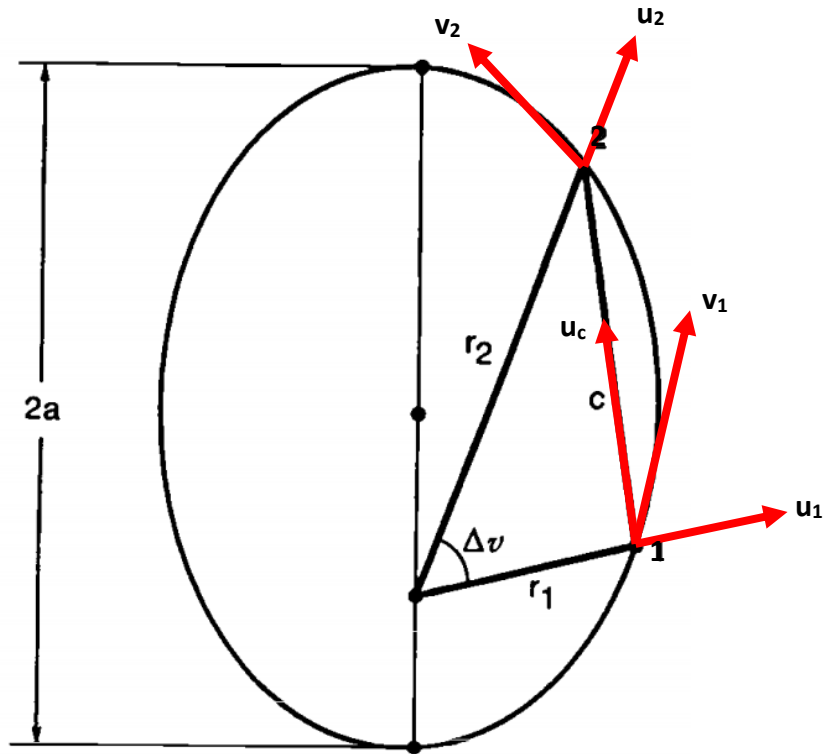


Figure 2.2. Lambert's Problem Diagram<sup>14</sup>

Next, the semiperimeter,  $s$ , can be easily found from

$$s = \frac{\|r_i\| + \|r_f\| + c}{2} \quad (2.16)$$

With the values  $c$  and  $s$ , the variables  $\alpha$  and  $\beta$  can be calculated as such

$$\alpha = 2 \sin^{-1} \left( \sqrt{\frac{s}{2a}} \right) \quad (2.17)$$

$$\beta = \pm 2 \sin^{-1} \left( \sqrt{\frac{s-c}{2a}} \right) \quad (2.18)$$

where  $\beta$  is negative if  $\Delta v$  is greater than  $180^\circ$ .<sup>12</sup> At this point, however,  $a$ , the semimajor axis of the transfer orbit is unknown. In order to minimize the maneuver time, the process must be iterated over increasing values  $a$  until the transfer time no longer decreases, starting with the minimum semimajor axis value

$$a_m = \frac{s}{2} \quad (2.19)$$

Then, iterating through the values of  $a$  and the corresponding  $\alpha$  and  $\beta$  values, the time-of-flight is found from

$$t_f = \sqrt{\frac{a^3}{\mu}} \{\alpha - \sin(\alpha) - [\beta - \sin(\beta)]\} \quad (2.20)$$

Now, the required  $\Delta V$  for the maneuver can be found. First, the velocity vectors at the beginning and the end of the transfer orbit must be calculated. A set of skewed unit vectors, as defined in Fig. 2.2, are determined to be

$$\mathbf{u}_1 = \frac{\mathbf{r}_1}{\|\mathbf{r}_1\|} \quad (2.21)$$

$$\mathbf{u}_2 = \frac{\mathbf{r}_2}{\|\mathbf{r}_2\|} \quad (2.22)$$

$$\mathbf{u}_c = \frac{\mathbf{r}_2 - \mathbf{r}_1}{c} \quad (2.23)$$

From these vectors, the velocity vector at the beginning of the transfer can be found from

$$\mathbf{v}_1 = (A + B)\mathbf{u}_c + (B - A)\mathbf{u}_1 \quad (2.24)$$

where

$$A = \sqrt{\frac{\mu}{4a}} \cot\left(\frac{\alpha}{2}\right) \quad (2.25)$$

$$B = \sqrt{\frac{\mu}{4a}} \cot\left(\frac{\beta}{2}\right) \quad (2.26)$$

Similarly, the velocity vector when departing the transfer orbit is

$$\mathbf{v}_2 = (A + B)\mathbf{u}_c - (B - A)\mathbf{u}_2 \quad (2.27)$$

The required  $\Delta V$  for the maneuver is then calculated using<sup>12</sup>

$$\Delta V = |\mathbf{v}_1 - \mathbf{v}_i| + |\mathbf{v}_2 - \mathbf{v}_f| \quad (2.28)$$

These two types of impulsive maneuvers have their limitations, though. A maneuver can only be assumed to be impulsive when the time allocated to perform the maneuver is significantly greater than the time spent thrusting. When this condition is not met, the thrust must be modeled as a finite burn.

When modeling a finite burn, the thrust is no longer assumed to occur at a single location, but is instead distributed throughout a finite length of time. As mentioned in the previous section, the spacecraft's position is propagated forward by integrating the equation of motion using MATLAB's ode45. When applying a finite burn, the equation of motion is changed slightly to include the acceleration due to the thrust

$$\mathbf{a} = -\frac{\mu}{\|\mathbf{r}\|^3} \begin{bmatrix} r_x \\ r_y \\ r_z \end{bmatrix} + \frac{T}{m} \begin{bmatrix} \sin(\alpha) \cos(\beta) \\ \cos(\alpha) \cos(\beta) \\ \sin(\beta) \end{bmatrix} \quad (2.29)$$

where  $T$  is the thrust,  $m$  is the mass, and  $\alpha$  and  $\beta$ , are the in-plane ( $\alpha$ ) and out-of-plane ( $\beta$ ) thrusting angles in the body-fixed RCN (radial-circumferential-normal) reference frame.

When integrating this equation at every time step, the mass use is determined by

$$\dot{m} = \frac{-T}{I_{sp}g} \quad (2.30)$$

where  $I_{sp}$  is the specific impulse and  $g$  is the acceleration due to Earth gravity. This means that the total spacecraft mass,  $m$ , in Eq. 2.23 changes at each time step. Additionally, the total  $\Delta V$  added due to the thrust can be calculated using

$$\Delta V = \frac{T/m}{1 + (\frac{m}{m})t} \quad (2.31)$$

where  $t$  is the total burn duration in seconds. This type of maneuver is used extensively in rapid collision avoidance.<sup>15</sup>

### 2.3 Orbital Regimes and Perturbations

No matter the type of maneuver performed, variations occur based on the orbital regime that the collision is predicted to occur in, which determines the perturbing forces acting on the spacecraft. In most scenarios, collision avoidance maneuvers will be necessary in a LEO or a Geostationary Earth Orbit (GEO). Spacecraft in LEO (altitudes between 160 and 2000 km) will see the highest changes in acceleration due to perturbing forces from atmospheric drag, oblateness (how non-spherical the Earth is), N-body accelerations (from the Moon and the Sun) and solar radiation pressure. Spacecraft in GEO (altitude of about 35,786 km), on the other hand, will primarily experience perturbations due to N-body forces (from the Moon and the Sun) and solar radiation pressure.

One method to apply these perturbations is through Cowell's method, where the acceleration due to the disturbances is added to the equations of motion during each numerical integrations step,

$$\mathbf{a} = -\frac{\mu}{\|r\|^3} \begin{bmatrix} r_x \\ r_y \\ r_z \end{bmatrix} + \mathbf{a}_p \quad (2.32)$$

where  $\mathbf{a}_p$  is the vector sum of all the perturbing accelerations to be included in the integration.<sup>14</sup>

The perturbing acceleration must then be calculated for each perturbing force. To find the perturbation due to the oblateness of the Earth, first the latitude of the spacecraft is found from the ECEF position using MATLAB's built-in `ecef2lla` function. Then, the position, latitude ( $\varphi$ ), and 70-by-70 tesseral and zonal coefficients ( $C$ , and  $S$ ) and potentials ( $P$ ) are used to determine the gravitational potential ( $U$ ) and its derivatives.

$$U = \sum_{i,j} \frac{\mu}{\|\mathbf{r}\|} P_{i,j} \sin(\varphi) \left( \frac{R_E}{\|\mathbf{r}\|} \right)^i C_z + \left( \frac{R_E}{\|\mathbf{r}\|} \right)^i P_{i,j} (C_t \cos(j\varphi) + S_t \sin(j\varphi)) \quad (2.33)$$

$$\frac{\partial U}{\partial r} = - \sum_{i,j} \frac{\mu}{\|\mathbf{r}\|^2} \left( \frac{R_E}{\|\mathbf{r}\|} \right)^i (i+1) P_{i,j} (C_t \cos(j\varphi) + S_t \sin(j\varphi)) \quad (2.34)$$

$$\frac{\partial U}{\partial \varphi} = \sum_{i,j} \frac{\mu}{\|\mathbf{r}\|} \left( \frac{R_E}{\|\mathbf{r}\|} \right)^i (P_{i,j} - j \tan(\varphi) P_{i,j}) (C_t \cos(j\varphi) + S_t \sin(j\varphi)) \quad (2.35)$$

$$\frac{\partial U}{\partial \lambda} = \sum_{i,j} \frac{\mu}{\|\mathbf{r}\|} \left( \frac{R_E}{\|\mathbf{r}\|} \right)^i j P_{i,j} (-C_t \sin(j\varphi) + S_t \cos(j\varphi)) \quad (2.36)$$

where  $R_E$  is the radius of the Earth,  $S_t$  and  $C_t$  are the tesseral values of  $S$  and  $C$ , respectively,  $C_z$  is the zonal component of  $C$ , and  $i$  and  $j$  correspond to the indices of the 70-by-70 matrices. Then, the derivatives of  $\mathbf{r}$ ,  $\varphi$ , and  $\lambda$  are found with respect to  $r$ .

$$\frac{\partial \mathbf{r}}{\partial r} = \frac{\mathbf{r}}{\|\mathbf{r}\|} \quad (2.37)$$

$$\frac{\partial \varphi}{\partial r} = \frac{1}{\sqrt{r_1^2 + r_2^2}} \left( -\frac{r r_3}{\|\mathbf{r}\|^2} + \frac{\partial r}{\partial r_3} \right) \quad (2.38)$$

$$\frac{\partial \lambda}{\partial r} = \frac{1}{\sqrt{r_1^2 + r_2^2}} \left( \mathbf{r}_1 \frac{\partial r}{\partial r_2} - \mathbf{r}_2 \frac{\partial r}{\partial r_1} \right) \quad (2.39)$$

The perturbing acceleration is now found from<sup>16</sup>

$$\mathbf{a}_{oblateness} = \frac{\partial U}{\partial r} \frac{\partial \mathbf{r}}{\partial r} + \frac{\partial U}{\partial \varphi} \frac{\partial \boldsymbol{\varphi}}{\partial r} + \frac{\partial U}{\partial \lambda} \frac{\partial \boldsymbol{\lambda}}{\partial r} \quad (2.40)$$

The next perturbation calculation, for drag, is much simpler. The acceleration due to drag is found simply from<sup>17</sup>

$$\mathbf{a}_{drag} = \frac{1}{2} \frac{C_d A}{m} \rho \|\mathbf{v}_{rel}\| \mathbf{v}_{rel} \quad (2.41)$$

where

$$\mathbf{v}_{rel} = \begin{bmatrix} \mathbf{v}_1 \\ \mathbf{v}_2 - \omega \mathbf{r}_1 \\ \mathbf{v}_3 \end{bmatrix} \quad (2.42)$$

in which  $\omega$  is the rotation rate of Earth in rads/sec,  $C_d$  is the coefficient of drag,  $A$  is the cross-sectional surface area in the ram direction, and  $\rho$  is the atmospheric density.

Calculating the acceleration due to N-body gravitational forces is equally simple. Given the position of the Sun and the Moon with respect to the Earth, the acceleration due to each individual body can be found using

$$\mathbf{a}_{nbody} = \mu_{body} \frac{\mathbf{r}_{body+r_{sc}}}{\|\mathbf{r}_{body+r_{sc}}\|^3} - \frac{\mathbf{r}_{body}}{\|\mathbf{r}_{body}\|^3} \quad (2.43)$$

where  $\mathbf{r}_{sc}$  is the radius vector between the spacecraft and the Earth and all vectors are defined in Fig. 2.3. Adding all of the accelerations due to each individual body gives the total acceleration due to all N bodies.

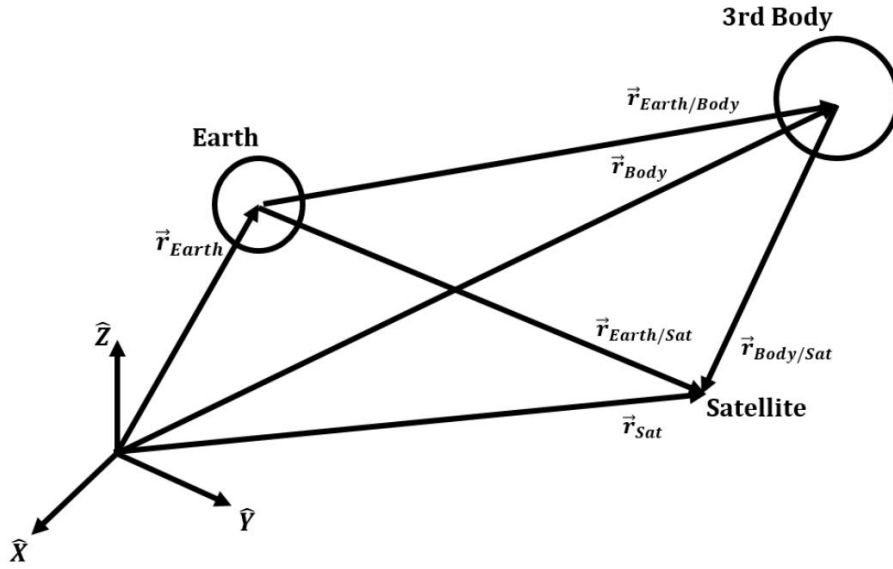


**Figure 2.3. N-Body Diagram**

The final perturbation, acceleration due to solar radiation pressure, can be assumed to be constant for this application since the distance between the spacecraft and the Earth is significantly smaller than the distance between the Sun and the Earth. The constant acceleration can then be found from

$$a_{SRP} = 4.65 \times 10^{-6} (1 - \beta) \frac{A}{m} \quad (2.44)$$

where  $\beta$  is the reflectivity of the spacecraft between 0 and 1 and  $A$  is the cross-sectional surface area of the spacecraft in the direction of the Sun. Combining the necessary accelerations (depending on the current altitude of the spacecraft) gives the total acceleration due to the perturbing forces.<sup>14</sup> Perturbative forces like these are the main source of uncertainty in the position of spacecraft in orbit and contribute in a large way to the collision avoidance problem.



## Chapter 3

### Collision Avoidance

While the orbital elements of spacecraft in orbit are typically published as TLEs (Two-Line Element Sets), there is always some uncertainty in each of these observations due to not only perturbations, but limitations on the capabilities of satellite-tracking ground stations. These uncertainties, if provided, come in the form of covariance matrices, which describe the error ellipsoids (standard deviation of position and velocity) of spacecraft. In collision avoidance, these standard deviation values are used to determine the maximum collision probability and the corresponding separation distance.

#### 3.1 Covariance

In describing the uncertainty of a satellite's position and velocity, a covariance matrix (the extent to which corresponding elements move in the same direction) provides all of the necessary data in the form

$$C = \begin{bmatrix} \sigma_x^2 & \rho_{xy}\sigma_x\sigma_y & \rho_{xz}\sigma_x\sigma_z & \sigma_{Vx}^2 & \rho_{VxVy}\sigma_{Vx}\sigma_{Vy} & \rho_{VxVz}\sigma_{Vx}\sigma_{Vz} \\ \rho_{yx}\sigma_y\sigma_x & \sigma_y^2 & \rho_{yz}\sigma_y\sigma_z & \rho_{VyVx}\sigma_{Vy}\sigma_{Vx} & \sigma_{Vy}^2 & \rho_{VyVz}\sigma_{Vy}\sigma_{Vz} \\ \rho_{zx}\sigma_z\sigma_x & \rho_{zy}\sigma_z\sigma_y & \sigma_z^2 & \rho_{VzVx}\sigma_{Vz}\sigma_{Vx} & \rho_{VzVy}\sigma_{Vz}\sigma_{Vy} & \sigma_{Vz}^2 \end{bmatrix} \quad (3.1)$$

where  $\sigma_x$ ,  $\sigma_y$ , and  $\sigma_z$  are the position standard deviations,  $\sigma_{Vx}$ ,  $\sigma_{Vy}$ , and  $\sigma_{Vz}$  are the velocity standard deviations, and  $\rho_{xy}$ ,  $\rho_{yx}$ ,  $\rho_{zx}$ ,  $\rho_{xz}$ ,  $\rho_{yz}$ , and  $\rho_{zy}$  are the correlation coefficients.

The corresponding covariance ellipsoids resemble that of those seen in Fig. 3.1. In hypervelocity encounters, the motion of the two ellipsoids can be assumed to be rectilinear (move in straight lines). This is what allows for collision probability to be solved for in conjunction (collision) scenarios.

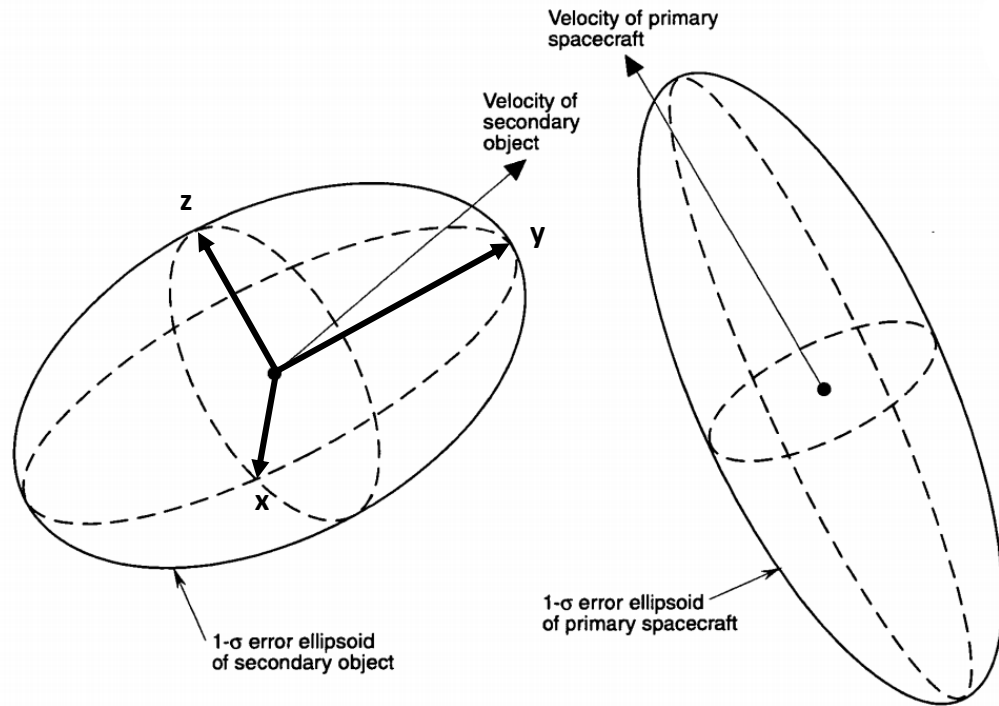


**Figure 3.1. Error Ellipsoids of Primary and Secondary Objects<sup>1</sup>**

### 3.2 Collision Probability and Separation Distance

The collision probability for any encounter is generally expressed as

$$P = \iiint_V f_3(x, y, z) dx dy dz \quad (3.2)$$

where

$$f_3(x, y, z) = \frac{1}{\sqrt{(2\pi)^3 |C|}} e^{-\frac{1}{2} r^T C^{-1} r} \quad (3.3)$$

is the Gaussian probability density function (pdf), in which  $r$  is the relative position of the primary object with respect to the secondary object and  $C$  is the combined covariance of the two objects. Then, by considering that the primary object crosses the encounter  $(x, z)$ -plane at the instant of closest approach, the pdf can be expressed in simply two dimensions.

$$f_2(x, z) = \frac{1}{2\pi\sigma_x\sigma_z\sqrt{1-\rho_{xz}^2}} e^{-\left[\left(\frac{x}{\sigma_x}\right)^2 - 2\rho_{xz}\left(\frac{x}{\sigma_x}\right)\left(\frac{z}{\sigma_z}\right) + \left(\frac{z}{\sigma_z}\right)^2\right]/2(1-\rho_{xz}^2)} \quad (3.4)$$

Next, an additional assumption is introduced. The problem can be simplified further assuming that the covariance is isotropic ( $\sigma_x$  and  $\sigma_z$  are equal – not  $\sigma_y$ ). This gives a new pdf

$$f(x, z) = \frac{1}{2\pi\sigma^2} e^{-\frac{(x^2+z^2)}{2\sigma^2}} \quad (3.5)$$

which makes the probability function over the area of the collision plane

$$P = \frac{1}{2\pi\sigma^2} \iint_{Area} e^{-\frac{(x^2+z^2)}{2\sigma^2}} dx dz \quad (3.6)$$

The lines of constant pdf are concentric circles with centers at the origin of the x-z plane and the cross-sectional area is an offset circle of radius  $r_A$  with its center at the point  $(x_e, 0)$  where  $x_e$  is the collision miss distance. Therefore, the probability can now be expressed as

$$P = \frac{1}{2\pi\sigma^2} \iint_{Area} e^{-\frac{[(x-x_e)^2+z^2]}{2\sigma^2}} dx dz \quad (3.7)$$

so now the lines of constant pdf are concentric circles with centers at the point  $(x_e, 0)$  and the cross-sectional surface area is a circle of radius  $r_A$  with its center at the origin. To eliminate the two variables,  $x$  and  $z$ , the probability can be expressed in terms of a single variable,  $r$ , instead as

$$P = \int_0^{r_A} \frac{r}{\sigma^2} e^{-(r^2+x_e^2)/2\sigma^2} I_0\left(\frac{rx_e}{\sigma^2}\right) dr \quad (3.8)$$

where the integrand is known as the Rician pdf and  $I_0(-)$  denotes the modified Bessel function of the first kind of order zero given by the infinite series<sup>1</sup>

$$I_0(\sqrt{\eta}) = \sum_{m=0}^{\infty} \frac{\left(\frac{\eta}{4}\right)^m}{(m!)^2} = 1 + \frac{\left(\frac{\eta}{4}\right)}{(1!)^2} + \frac{\left(\frac{\eta}{4}\right)^2}{(2!)^2} + \frac{\left(\frac{\eta}{4}\right)^3}{(3!)^2} + \dots \quad (3.9)$$

The probability can also be written more simply as

$$P = \frac{1}{2v} e^{-v/2} \int_0^{\eta_A} e^{-\eta/2v} I_0(\eta) d\eta \quad (3.10)$$

where

$$\eta = \left(\frac{rx_e}{\sigma^2}\right)^2 > 0 \quad (3.11)$$

$$\eta_A = \left(\frac{r_A x_e}{\sigma^2}\right)^2 > 0 \quad (3.12)$$

$$u = \left(\frac{r_A}{\sigma}\right)^2 > 0 \quad (3.13)$$

$$v = \left(\frac{x_e}{\sigma}\right)^2 > 0 \quad (3.14)$$

If we substitute the convergent infinite series Eq. (3.9) into Eq. (3.8), we obtain

$$P = \frac{1}{2v} e^{-v/2} \sum_{m=0}^{\infty} \frac{1}{4^m (m!)^2} \int_0^{\eta_A} \eta^m e^{-\eta/2v} d\eta \quad (3.15)$$

Defining  $J_m$  conveniently as

$$J_m = \int_0^{\eta_A} \eta^m e^{-\eta/2v} d\eta \quad (3.16)$$

it may be shown that

$$J_m = m! (2v)^{m+1} \left(1 - e^{-\frac{u}{2}} \sum_{k=0}^m \frac{u^k}{2^k k!}\right) \quad (3.17)$$

which then gives

$$P = e^{-v/2} \sum_{m=0}^{\infty} \frac{v^m}{2^m m!} \left(1 - e^{-u/2} \sum_{k=0}^m \frac{u^k}{2^k k!}\right)$$

If only the first term in the series is used ( $m = 0$ ), then we have the expression

$$P = e^{-v/2} (1 - e^{-u/2}) \quad (3.18)$$

which gives results to within three or four significant digits of accuracy under a wide range of input collision parameters, including cases where  $\sigma_x$  and  $\sigma_z$  are not equal.

Inverting this equation gives the “nominal” miss distance in terms of the desired collision probability

$$x_e = \sigma^* \sqrt{2 \ln \left( 1 - e^{-\frac{r_A^2}{2\sigma^2}} \right) - \ln(P)} \quad (3.19)$$

in which

$$\sigma^* = \sqrt{\sigma_{z'}^2 \left( 1 + \left( \frac{\sigma_{z'}}{\sigma_{x'}} \right)^2 - 1 \right) \cos^2 \theta}^{-1} \quad (3.20)$$

where  $\delta$  is the rotational angle between the coordinate system and the principal directions

$$\delta = \frac{1}{2} \tan^{-1} \left[ \frac{2\rho_{xz}\sigma_x\sigma_z}{(\sigma_x^2 - \sigma_z^2)} \right] \quad (3.21)$$

which, after rotation, makes the covariance matrix

$$C' = \begin{bmatrix} \sigma_{x'}^2 & 0 \\ 0 & \sigma_{z'}^2 \end{bmatrix} \quad (3.22)$$

where the standard deviations of the two frames are related by

$$\sigma^2 = \sigma_{x'}\sigma_{z'} = \sqrt{1 - \rho_{xz}^2} \sigma_x \sigma_z \quad (3.23)$$

In the case that  $\theta = 0$  (assumed throughout the remainder of the paper),  $\sigma^*$  becomes

$$\sigma^* = \sqrt{\sigma_z^2 \left( 1 + \left( \frac{\sigma_z}{\sigma_x} \right)^2 - 1 \right)}^{-1} \quad (3.24)$$

thus providing a relationship between the “nominal” separation distance and the desired collision probability for both isotropic and nonisotropic probability density functions.<sup>1</sup>

This will prove useful in Chapters 4 and 5 when optimizing the avoidance maneuver for various desired collision probabilities.

## **Chapter 4**

### **Optimizing The Maneuver**

A numerical solution relating the desired collision probability and the required thrust duration can be found by optimizing the thrusting direction and location that results in the lowest amount of fuel to reach the desired separation distance (or maximum collision probability). The optimization of the rapid collision avoidance maneuver relies on the complexities that arise from applying finite burn analysis while choosing burn locations and directions uncharacteristic of long-duration maneuvers. With these in mind the numerical solution can be transformed into a semi-analytical solution to the problem. First, a numerical solution must be found. This relies on the optimization of three parameters: thrust location, coast location, and thrust direction.

#### **4.1 Thrust Location**

A primary complexity that arises from these minimal time-to-collision maneuvers is the optimal location of the burn. When a longer time is allotted for the avoidance maneuver, the burn will always be placed at perigee or apogee, the most efficient locations in an elliptical orbit to perform a maneuver.<sup>13</sup> However, when less time than half-an-orbit is available to perform the maneuver, thrusting at perigee or apogee may not

be an option, so a less optimal thrust location may be necessary. This results, unfortunately, in a greater  $\Delta V$  and, thus, a longer burn time to complete the maneuver.

To determine an optimal location to perform the maneuver, a “wait time” parameter is applied. If the required burn time is less than the available time to perform the maneuver, then some flexibility is allowed in where thrust is applied. To lower the time spent thrusting, the “wait time” is placed at the beginning of the maneuver to ensure that the majority of the thrusting occurs at the most efficient point in the remaining orbit arc before the collision was predicted to occur. If perigee or apogee are between the notification epoch and the predicted collision location, then the “wait time” is applied such that the maneuver is centered around this optimal location.

## **4.2 Coast Location**

Once the beginning of the thrust location is chosen based on the “wait time,” a second non-thrusting coast period can be added after the burn occurs. If, after applying the “wait time”, thrusting the remaining time-to-collision causes the spacecraft to exceed the desired minimum separation distance, then a coast phase can be applied after the burn to decrease the separation distance at the collision location. The coast location is chosen such that the combined time of the thrust duration and the two coast periods results in the spacecraft reaching exactly the desired separation distance at the predicted collision location.



### 4.3 Thrust Direction

The third optimization parameter is the direction in which the thrust is applied. Luckily, the complexity of optimizing the thrust direction becomes a simplification in this case. The angles,  $\alpha$  and  $\beta$ , are the in-plane ( $\alpha$ ) and out-of-plane ( $\beta$ ) thrusting angles in the body-fixed RCN (radial-circumferential-normal) reference frame. This reference is such that the radial component is aligned with the radial unit vector positive in the zenith direction, the normal component is aligned with the osculating angular momentum vector positive and the circumferential component is normal to the radius vector in the orbital plane and completes the right-handed triad of unit vectors, as seen in Figure 4.1.

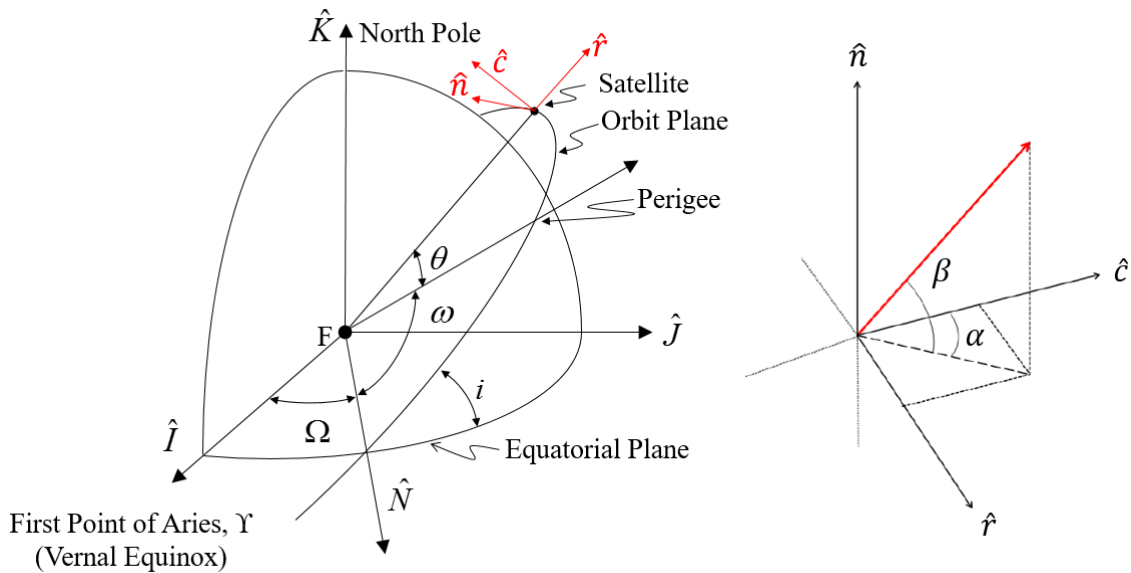


**Figure 4.1. Left: RCN reference frame with respect to the Central-Body-Centered inertial reference frame (IJK). Right:  $\alpha$  and  $\beta$  thrust angles with respect to the RCN reference frame.**

With the thrust location known, the optimal in-plane and out-of-plane angles can be chosen to minimize the duration of the burn. Considering all possible thrust locations, spacecraft parameters, and orbit orientations in Low-Earth Orbit, an optimal burn direction was chosen for each maneuver which required the least amount of time spent burning. It turns out that, when the burn duration is shorter than approximately 90 minutes (about the time to complete one orbit in LEO), the optimal burn duration is always radial ( $90^\circ$  from the velocity vector) in the in-plane axis ( $\alpha$ ) and along the velocity vector direction in the out-of-plane axis ( $\beta$ ). This simplification, assuming a radial thrusting direction going forward, is what allows for the analytical solution to be formed.

Though the thrust direction is always assumed to be radial, the binary switch between thrusting along the direction of the position vector or in the reverse direction is determined based on the instantaneous velocity vectors of both the primary and secondary objects. If the angle between the two vectors (determined using the law of cosines) is between  $0$  and  $180^\circ$ , the thrust is performed along the direction of the position vector. Otherwise, if the angle is between  $180^\circ$  and  $360^\circ$ , the thrust is performed in the reverse direction of the position vector. This ensures that the maneuver cannot increase the probability that a collision will occur between the two objects at a different point in time before or after the predicted collision.

#### 4.4 Numerical Method Optimization

With the three optimization parameters defined, the method in which they are chosen can be explained in further detail. This leads to the final complexity: finite burn modeling. When rapid collision avoidance maneuvers are necessary, the time-to-collision is not significantly greater than the time spent burning to complete the maneuver. This means that the burn can no longer be assumed to be impulsive. Instead, finite burn analysis must be used, where the burn is integrated (including fuel mass loss) with the position and velocity of the spacecraft at every time step in the propagation. Comparing the two methods, it was found that performing short duration maneuvers with the impulsive burn assumption (performed at the notification epoch) resulted in separation distance values over 460% greater than if a finite burn were applied for the entire time-to-collision duration (Fig. 4.2). The large difference between the two distances, and the fact that finite burn analysis is considered to be the more accurate of the two methods, means that the impulsive burn assumption can no longer be made.

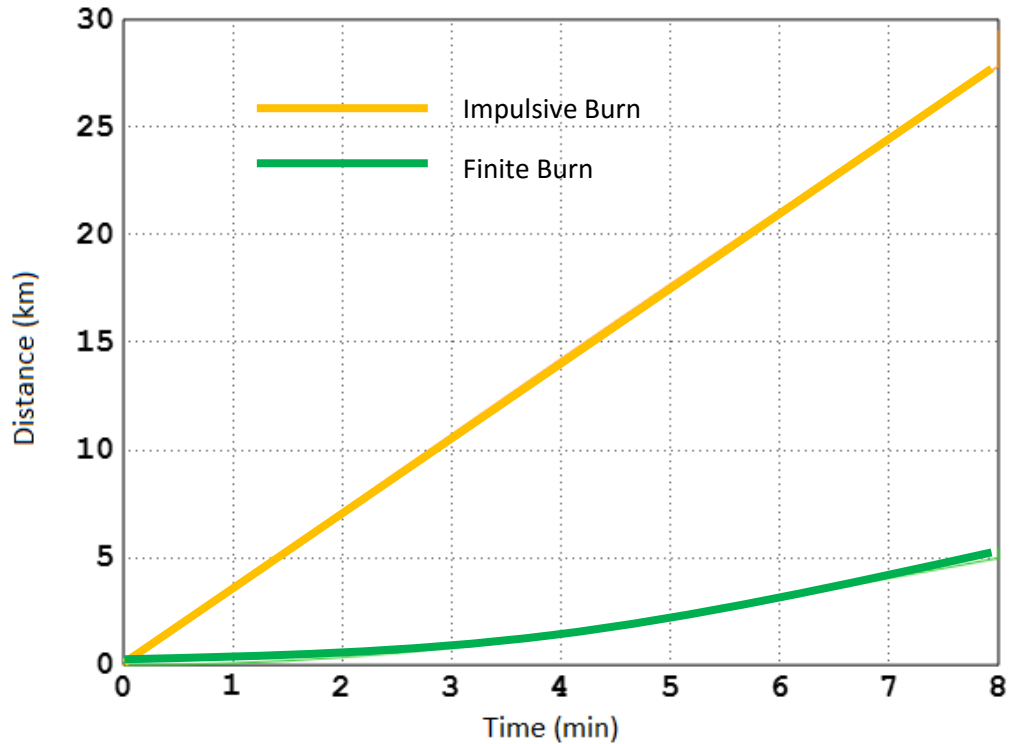


**Figure 4.2. Separation Distance vs. Burn Duration for Impulsive and Finite Burn Maneuvers in Low-Earth Orbit**

Now that all of the assumptions are accounted for, the position and velocity of the spacecraft can be propagated forward in the arc between the notification epoch and the predicted collision location using finite burn modeling applied in MATLAB's ode45. Propagating the orbit with a variable time-step solver like ode45 allows for larger steps to be taken when allowed and smaller time steps to be taken when required by the solution. This ensures that the orbit propagation is as accurate as possible with relative and absolute tolerances set to  $1 \times 10^{-6}$ . In collision avoidance scenarios with larger time frames, the fidelity of the orbit propagator would be an issue. However, with such minimal time-to-collision values, the orbit isn't propagated long enough for any perturbations such as drag and oblateness to affect the position and velocity of the spacecraft (see Section 4.5).

The optimal thrusting duration is determined by propagating the spacecraft’s orbit as such while iterating through all possible “wait time” and coast time values. The first step in each iteration is to propagate the nominal trajectory forward for the “wait time” duration. Subtracting the “wait time” and coast time from the time-to-collision, the thrust duration is found to be the time remaining in the maneuver. The spacecraft’s position is then propagated further for the thrust duration while applying the finite burn. Finally, the position is once again propagated (without the finite burn) for the coast time. The resulting position vector is then compared to the position of the secondary body at the time of the collision to determine the separation distance. After iterating through all possible wait time and coast time options, the “wait time” and coast time values can be found that result in the desired separation distance being achieved while also minimizing the necessary burn time to do so. This iteration process can be seen summarized in the flowchart in Figure 4.3.

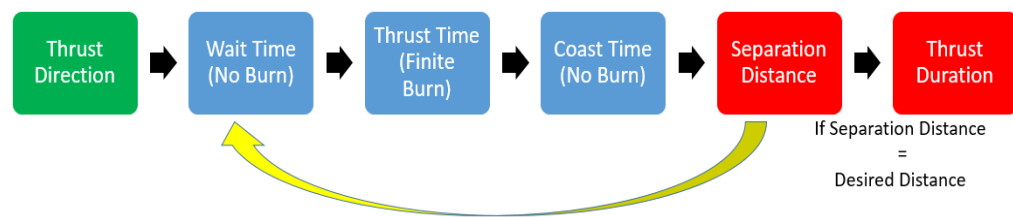


**Figure 4.3. Optimization Flow Chart to the Minimal Thrust Duration That Achieves the Desired Separation Distance**

Once the minimized thrust duration and the resulting separation distance is known, a relationship between the thrust duration and maximum collision probability can be developed. Given the nature of the collision avoidance problem, using a desired collision probability is typically preferred over the separation distance. Luckily, a

relationship, originally stated in Eq. 3.19 earlier, (assuming a high relative velocity between the two colliding objects) between the two exists:<sup>1</sup>

$$d = \frac{1}{1000} \sigma^* \sqrt{2 * \ln \left( 1 - e^{-\frac{r_A^2}{2 * \sigma^2}} \right) - \ln(P_{max})} \quad (4.1)$$

in which

$$\sigma = \sqrt{\sigma_x \sigma_z} \quad (4.2)$$

and

$$\sigma^* = \sqrt{\sigma_z^2 \left( 1 + \left( \left( \frac{\sigma_z}{\sigma_x} \right)^2 - 1 \right) \right)^{-1}} \quad (4.3)$$

which simplifies to

$$\sigma^* = \sigma_x \quad (5.4)$$

where  $\sigma_x$  and  $\sigma_z$  are the covariance in the  $x$  and  $z$  axis,  $r_A$  is the combined radius of the two bodies, and  $P_{max}$  is the maximum allowed collision probability. With the separation distance known, the corresponding maximum collision probability can be calculated from the two-dimensional covariance of the spacecraft (as discussed in Chapter 3) and the combined radius of the spacecraft and secondary object. This gives a relationship between the thrust direction and the maximum collision probability, which is the desired correlation.

## 4.5 Effect of Perturbations

In propagating a spacecraft's trajectory, whether applying thrust or not, the acceleration due to perturbative forces must be taken into account. However, when propagating for such short periods of time, the perturbations will have less of an effect on the final position of the spacecraft at the predicted collision time. This was put to the test by propagating a spacecraft's orbit a full period prior to a predicted collision with a desired separation distance of up to 10 km. It was found that the perturbed trajectory varied from the unperturbed trajectory by only 0.3463%. This means that, for all rapid collision avoidance maneuvers in Low-Earth Orbit, the perturbing forces can be assumed to be insignificant and the trajectories can be propagated without perturbations. Maneuvers in GEO, on the other hand, are long enough in duration that perturbations must be included. The lack of necessity to include perturbations in LEO quick response avoidance maneuvers is what allows for an analytical solution to be found, as described in the coming chapter.

## Chapter 5

### Analytical Method

With minimal time-to-collision, every second that goes into planning and executing the avoidance maneuver could mean the difference between colliding with the secondary object and avoiding it. One of the biggest hurdles in speeding up the process is the time spent calculating the optimal maneuver. Fortunately, an analytical solution could mean a computation time of fractions of a second for any desired rapid collision avoidance maneuver.

With the problem simplified due to the radial thrusting assumption, the variables were then limited to the spacecraft location and time-to-collision. It was determined that time-to-collision values up to half-an-orbit produced linear separation distance vs. thrusting duration curves. However, limiting the time-to-collision to between 6 and 16 minutes (assuming a constant acceleration of  $0.2 \text{ km/s}^2$ ) resulted in the most realistic best-fit coefficients given the computing resources available. Using the range of values shown in Table 5.1, a multiple linear regression technique was applied to determine an analytic equation that can be used to solve for the required thrusting duration for any of the sample scenarios.



**Table 5.1.** Valid Range of Inputs for the Analytical Solution

Variable	Minimum Value	Maximum Value
Semimajor Axis (a)	6778.137 km	8378.137 km
Eccentricity (e)	0	0.5
True Anomaly ( $\theta$ )	0	$\pi$
Time-to-Collision ( $t_{\text{coll}}$ )	6 minutes	16 minutes

The multiple linear regression technique<sup>19</sup> uses the least squares method to find a line-of-best-fit by minimizing the sum of the squares of the vertical distance from each data point on the line. The general model for  $k$  variables is of the form

$$y_i = \beta_0 + \beta_1 x_{i1} + \beta_2 x_{i2} + \beta_3 x_{i3} + \dots + \beta_k x_{ik} + e_i, \quad i = 1, 2, \dots, n \quad (5.1)$$

The regression coefficients,  $\beta$ , can best be estimated by writing the set of equations using matrix notation. The model then takes the form

$$Y = X\beta + \epsilon \quad (5.2)$$

which can be written in matrix notation as

$$\begin{bmatrix} y_1 \\ y_2 \\ y_3 \\ \dots \\ y_n \end{bmatrix} = \begin{bmatrix} 1 & x_{11} & \dots & x_{1k} \\ 1 & x_{21} & \dots & x_{2k} \\ \dots & \dots & \dots & \dots \\ 1 & x_{n1} & \dots & x_{nk} \end{bmatrix} \begin{bmatrix} \beta_1 \\ \beta_2 \\ \beta_3 \\ \dots \\ \beta_n \end{bmatrix} + \begin{bmatrix} \epsilon_1 \\ \epsilon_2 \\ \epsilon_3 \\ \dots \\ \epsilon_n \end{bmatrix} \quad (5.3)$$

where each column of  $x$  values corresponds to each of the independent variables in Table 5.1. The values for  $\beta$  can be found by solving the least square normal equation

$$X^T X \hat{\beta} = X^T Y \quad (5.4)$$

which gives

$$\hat{\beta} = (X^T X)^{-1} X^T Y \quad (5.5)$$

Since the thrusting duration varies significantly with time-to-collision variables, the multiple linear regression process described above was used to find best-fit equations for sets of different values within the ranges in Table 5.1. While exploring the multiple linear regression processes, it was found that including quadratic terms for each of the independent variables actually produced a tighter fit from the resulting regression equations, such as

$$\begin{aligned} t_{burn} = & -4.9719 - 7.3236x10^{-4} a + 8.9180x10^{-7} a^2 - 3.1658 \theta - 2.0152 \theta^2 \\ & - 0.3925 t_{coll} - 0.0310 t_{coll}^2 - 9.9438 e - 19.8876 e^2 \\ & + 6.6808 d + 0.0584 d^2 \end{aligned} \quad (5.6)$$

A second round of multiple linear regression was then used on each set of regression coefficients to determine a single relationship, seen in Eq. (5.7), between the inputs and the required thrust duration. The second round of multiple regression was used in order to reduce the error between the numerically calculated thrust durations and the analytic equation.

$$\begin{aligned} t_{burn} = & 5.3663 - 2.753x10^{-4} a + 8.3244x10^{-7} a^2 + 3.0872 \theta - \\ & 1.3993 \theta^2 - 0.3469 t_{coll} - 0.1382 t_{coll}^2 + 19.8018 ecc + \\ & 61.6356 ecc^2 + 16.5308 d + 0.5159 d^2 + (-0.0020 - 1.3537x10^{-7} a - \\ & 6.2518x10^{-13} a^2 - 5.8562x10^{-4} \theta - 3.0945x10^{-4} \theta^2 - \\ & 2.0311x10^{-4} t_{coll} - 2.3422x10^{-5} t_{coll}^2 - 0.0037 ecc - 0.0130 ecc^2 - \\ & 5.6449x10^{-5} d + 2.7438x10^{-5} d^2) a + (0.6960 + 9.1342x10^{-5} a + \\ & 1.2078x10^{-8} a^2 - 0.6966 \theta - 0.2217 \theta^2 + 0.0737 t_{coll} + 0.0089 t_{coll}^2 + \\ & 1.0310 ecc + 3.4434 ecc^2 + 0.3623 d - 0.0350 d^2) \theta + (-0.0034 + \\ & 7.4799x10^{-7} a + 1.4032x10^{-10} a^2 - 0.0026 \theta - 0.0015 \theta^2 + \\ & 0.0775 t_{coll} + 0.0175 t_{coll}^2 - 0.0179 ecc - 0.0314 ecc^2 - 0.7981 d - \\ & 0.0459 d^2) t_{coll} + (4.7952 + 6.2801x10^{-4} a + 8.2903x10^{-8} a^2 + \\ & 1.1814 \theta + 0.6250 \theta^2 + 0.5191 t_{coll} + 0.0640 t_{coll}^2 - 27.1348 ecc - \\ & 54.1805 ecc^2 - 1.2987 d + 0.2203 d^2) ecc \end{aligned} \quad (5.7)$$

Each constant in Eq. (5.7) is the regression coefficient representing the correlation between the two independent variables in the term and their combined effect on the necessary burn time. Then, this relationship can be expressed in terms of maximum probability of the collision by substituting the relationship in Eq. (4.1) for each  $d$  variable. For this expression, the covariance data for the position of the primary object must be known. Assuming an isotropic covariance distribution as in Chapter 3, the covariance in the  $z$  and  $x$  directions can be assumed to be equivalent. Then, the two covariance values and the combined radii of the two objects can be used along with the separation distance to determine a relationship for the maximum collision probability. If the covariance of the primary object is unknown, the covariance in both directions can be assumed to be between 1 and 10 km (in LEO) and the combined radius can be safely taken up to 100 m.<sup>1</sup>

## **Chapter 6**

### **Trade Studies**

One key component of the mission design process is the use of trade studies. A trade study, by definition, is an objective comparison with respect to performance, cost, schedule, risk, and all other reasonable criteria of all realistic alternative requirements; architectures; baselines; or design, verification, manufacturing, deployment, training, operations, support, or disposal approaches. Trade studies support requirements development, system architecture development, system synthesis (assess the impact of alternative performance), assessing proposed design changes, and make/buy decisions. The whole process occurs in seven steps, as outlined in Fig. 6.1. First, the problem is established by determining the problem statement, requirements and constraints, and the desired level of detail in the analysis. Then, the requirements and constraints are reviewed for completeness and conflicts while communication is established with the customer. Third, the trade-off methodology is determined as well as the criteria and the corresponding weighting system. Next, all alternatives are identified and the viable candidates for the study are selected. Then, the models are developed to measure the merit of each design and the values are assigned to each candidate. The results are then analyzed by calculating the relative value based on the chosen methodology, evaluating the alternatives, performing a sensitivity analysis, and selecting the preferred alternative. Finally, the results from the study are documented.

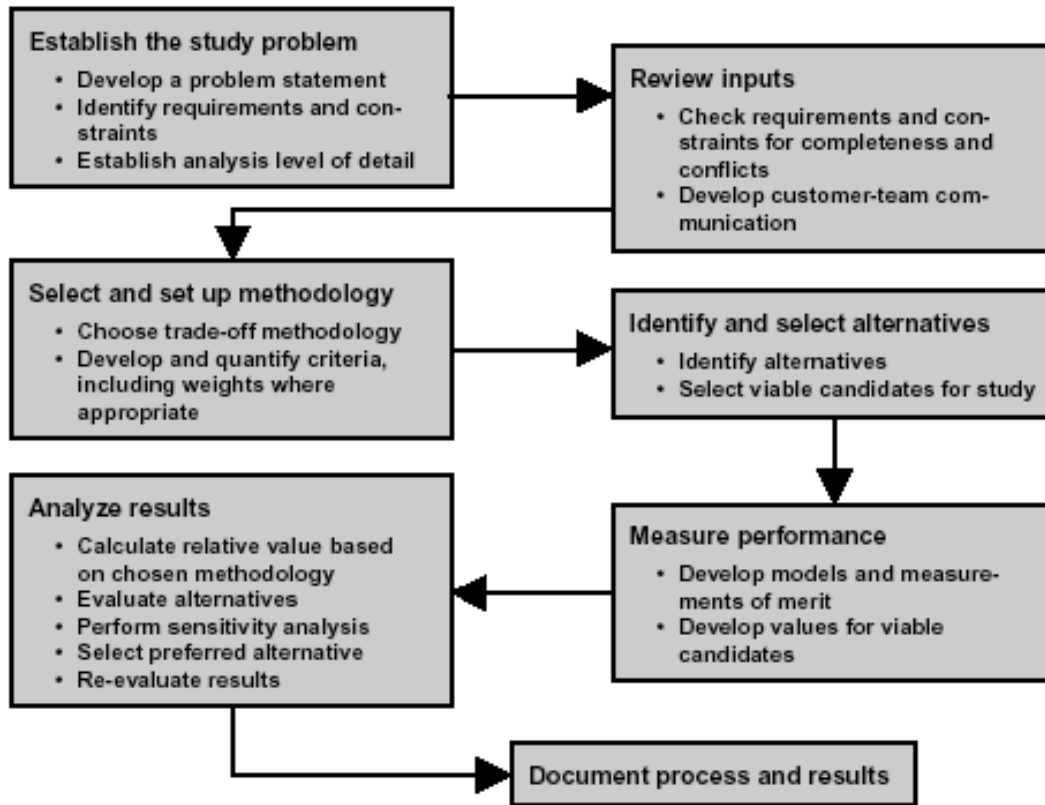



**Figure 6.1. Seven Step Trade Study Process**

Performing a trade study depends on comparing criteria for making decisions, such as the measures of effectiveness and the measures of performance. A measure of effectiveness is a measure of how well mission objectives are achieved, such as life cycle cost, mission duration, technology readiness level (TRL), crew capacity, and payload mass. A measure of performance is a quantitative measure that will help ensure that a measure of effectiveness is met, such as mass, power consumption, specific impulse, and propellant type. Both the measures of effectiveness and measure of performance are used to determine the merit of a design. One must be careful to limit the number of designs and measures under consideration, and, if possible, a baseline solution should be established for comparison of alternatives. Though trades are usually subjective, and one

must be careful about falling into a false sense of accuracy, trade studies are valuable in weighing the benefits of drawbacks of various designs and choosing the preferred option.

In order to do so, a trade study decision matrix is created (as in Fig. 6.2, a matrix example for batteries). In the far left column are the criteria, including both the measures of effectiveness and the measures of performance. To the right of that are the two columns used for setting the consequence of each criteria: whether or not they are mandatory and a weighting (adding to 100% for all criteria). Each of the far right columns is used for evaluating all possible design choices for each of the criteria, assigning each choice a score between one and three, where three is the most preferred. Multiplying each score by the weighting of that row and summing each column gives a single value between 0 and 100 for each design solution. The highest value, in this case corresponding to “Collect Experiment Data with Alternative Experiment”, is the preferred solution.

Decision Matrix Example for Battery			ENTER SCORES 	Extend Old Battery Life	Buy New Batteries	Collect Experiment Data With Alternative Experiment	Cancelled Experiment
CRITERIA	Mandatory (Y=1/N=0)?	Weight	SCALE				
Mission Success (Get Experiment Data)	1	30	3 = Most Supportive 1 = Least Supportive	2	3	3	0
Cost per Option	0	10	3 = Least Expensive 1 = Most Expensive	1	2	3	1
Risk (Overall Option Risk)	0	15	3 = Least Risk 1 = Most Risk	2	1	2	3
Schedule	0	10	3 = Shortest Schedule 1 = Longest Schedule	3	2	1	3
Safety	1	15	3 = Most Safe 1 = Least Safe	2	1	2	3
Uninterrupted Data Collection	0	20	3 = Most Supportive 1 = Least Supportive	3	1	2	1
WEIGHTED TOTALS in %		100%	3	73%	60%	77%	0%

**Figure 6.2. Example Trade Study Decision Matrix**

After performing a trade study, all that is left is a reality check on the solution. It may turn out that all requirements and constraints have not been met or that the solution doesn't hold up under a wide range of input values. Once these both have been verified, and all subjective aspects of the problem have been fully addressed, the robustness of the solution can be tested by exploring the full reasonable range of each performance variable to understand the domain where the selected solution is appropriate. Trade studies, as described above, will prove useful in determining the best collision avoidance maneuver and return trajectory when considering the impact of the maneuver on mission performance.<sup>18</sup>

## Chapter 7

### Trading A Complete Trajectory

With the avoidance maneuver optimized both numerically and analytically, the return trajectory to the nominal orbit can be solved as well. As discussed in Chapter 2, minimum-fuel Hohmann transfers and the minimum-time Lambert's problem were considered for the return. A trade study can be conducted comparing the minimum-fuel transfer, minimum-time transfer, and minimum-probability cases to determine the desired return trajectory given the weights provided for each metric by the mission designers.

#### 7.1 Return Trajectories

In the case of the Hohmann transfer, the spacecraft would remain on its post-collision orbit until it reaches perigee and then would commence a Hohmann transfer to arrive on the original orbit at apogee. While this transfer will always require the least amount of fuel to perform, it also takes significantly longer than the minimum-time Lambert's problem. As is to be expected, solving for a perigee-to-apogee ( $180^\circ$ ) Lambert's problem transfer gives the same required  $\Delta V$  and time-of-flight as the Hohmann transfer. This means that all possible transfers, despite the desired optimization parameter(s), can be solved for using Lambert's problem by varying the time-of-flight.



In order to explore all possible return trajectory options, Lambert's problem is solved for all possible departure locations (where after the predicted collision location the spacecraft departs from the post-collision orbit), all arrival locations on the nominal orbit, and all return maneuver durations (up to one orbital period in duration). The required  $\Delta V$  for all possible transfers was found for all combinations of departure location, arrival location, and maneuver duration values. However, as demonstrated in Chapter 4, the impulsive maneuver assumption made for Lambert's problem is not valid for the majority of the minimum-time transfer options. This requires two adjustments to be made in order to ensure accurate  $\Delta V$  values and realistic return trajectory options.

First, the initial avoidance maneuver is recreated assuming an impulsive Lambert's problem burn for all possible maneuver durations up to one orbital period in length. These values are then divided into the actual required  $\Delta V$  values for the avoidance maneuver to get a relationship between the impulsive and finite burn values. This relationship is then used to determine the actual required  $\Delta V$  for the possible return trajectories. The second adjustment is to ensure that the  $\Delta V$  required can actually be accomplished in the allotted maneuver duration. Given the relationship between the burn duration and the  $\Delta V$  of the avoidance maneuver, it can be determined how long it takes to impart the required  $\Delta V$  into the return trajectory. If the calculated burn duration is greater than the allotted maneuver duration, then that trajectory is considered to no longer be a valid option. The remaining trajectories are then compared for their corresponding  $\Delta V$  values and maneuver durations, and the process is repeated for each desired separation distance/ collision probability value. The resulting relationship between maximum allowed collision probability,  $\Delta V$ , and maneuver duration are the basis for the trade study.

## 7.2 Trade Study Metrics and Weights

When designing a satellite mission, many factors are considered related to the health of the spacecraft, the cost of launching it and its fuel reserves into space, and the sensitivity of the nominal orbit to perturbations and course corrections. In Low-Earth Orbit, for example, the orientation and location of the spacecraft can have a significant impact on its ability to meet the prescribed mission requirements. In addition, in order to minimize the launch mass of the spacecraft, only a minimal amount of extra fuel is included for unplanned maneuvers. This means that any avoidance maneuver must be carefully considered given the likelihood of collision (a measure of effectiveness), the time spent away from the nominal orbit (a measure of performance), and the amount of fuel (proportional to the  $\Delta V$ ) required to perform the maneuver (a measure of performance). These three values are used as metrics when weighing the avoidance maneuver and return trajectory options and deciding on a preferred course of action.

With thousands of options available to return the spacecraft to the nominal orbit, a trade study is necessary to narrow down and compare the possibilities. In narrowing down the options to be compared, a maximum of three options were considered at one time: the minimum fuel case, the minimum time case, and/or the minimum collision probability case. Given that the weighting applied to each of these, as discussed in Chapter 6, is largely dependent on the design of the mission, the availability of fuel onboard the spacecraft, and the imminence of the predicted collision, multiple trade studies must be conducted in order to determine the best course of action under various conditions. In comparing the trade studies, patterns can be noted, such as the effect of the

notification time on the feasibility of the maneuvers. Patterns such as this can be used to make suggestions to the mission designers in the preliminary design stage. As collisions are predicted to occur, engineers involved in the operation of the spacecraft can use the same trade studies with their own desired weights and limitations applied to the metrics to determine the ideal course of action to avoid – or risk colliding with – the approaching object. The results of these trade studies and subsequent recommendations for use in future collision avoidance operations are summarized in the following chapter.

## **Chapter 8**

### **Results**

#### **8.1 The Analytical Solution**

With a single relationship between the desired collision probability (or desired separation distance) and required thrust duration, the semi-analytical solution can now be compared to the numerical solution presented earlier. For all data in Table 5.1 used to generate the semi-analytical solution, the required thrust duration to reach the desired separation distance was calculated.

Comparing these results to those of the numerical solution used to produce the semi-analytical equation, the average error was found to be less than 30%. Significantly lower errors are possible, though, under two conditions. First, a limited number of cases from Table 5.1 were used to produce the best-fit coefficients. Including more data would produce much closer fits with less error between the numerical and analytical solutions. In addition, with a priori knowledge of the mission such as valid ranges of semimajor axis and eccentricity values, even tighter fits could be produced, down to significantly less than a 5% error, so 30% is easily a worst case scenario. Knowing and accounting for

the maximum error when calculating the required thrust duration can ensure that all collisions are successfully avoided as necessary.

Now, the solution can be narrowed down to a generic test case to demonstrate the accuracy of the analytical solution compared to the numerical solution. Assuming a spacecraft with a mass of 1000 kg and a thrust of 200 N in a 700 km circular orbit inclined at  $0^\circ$ , the thrust duration can be found for a time-to-collision of 6 minutes. Using the analytical expression from Eq. (5.7), a plot demonstrating the relationship between the optimal thrust duration and the desired separation distance (Fig. 8.1) can be generated comparing the numerical and analytical solutions. At the desired separation distance of five kilometers, the error for this case is found to be 13.01%.

Given the analytical relationship between the thrust duration and separation distance, the maximum collision probability can be calculated with only additional knowledge on the size of the two objects and the uncertainty in the position of the primary object. For this generic test case, with no real covariance data, the covariance in both the  $x$  and  $z$  directions is assumed to be 5 km, with a combined radii of 10 m. Plugging these values into Eq. (4.1) gives a single relationship between the separation distance and the maximum collision probability. This can then be used, in combination with the analytical relationship from Eq. (5.7), to give a single relationship between the maximum collision probability and the optimal burn duration. Using this relationship for the generic test case gives the relationship between the two variables, as seen in Fig. 8.2 comparing the numerical and analytical results.

Comparing Figures 8.1 and 8.2, it can be observed that, although the relationship between thrust duration and the desired separation distance is linear for the cases tested,

this can be used to determine a non-linear solution calculating the fuel-optimal thrust duration from the desired maximum collision probability. Given the variation in the position and velocity of both objects due to errors in object observations, the level of accuracy to which the thrust duration can be determined from the collision probability is well within the necessary levels for this application.

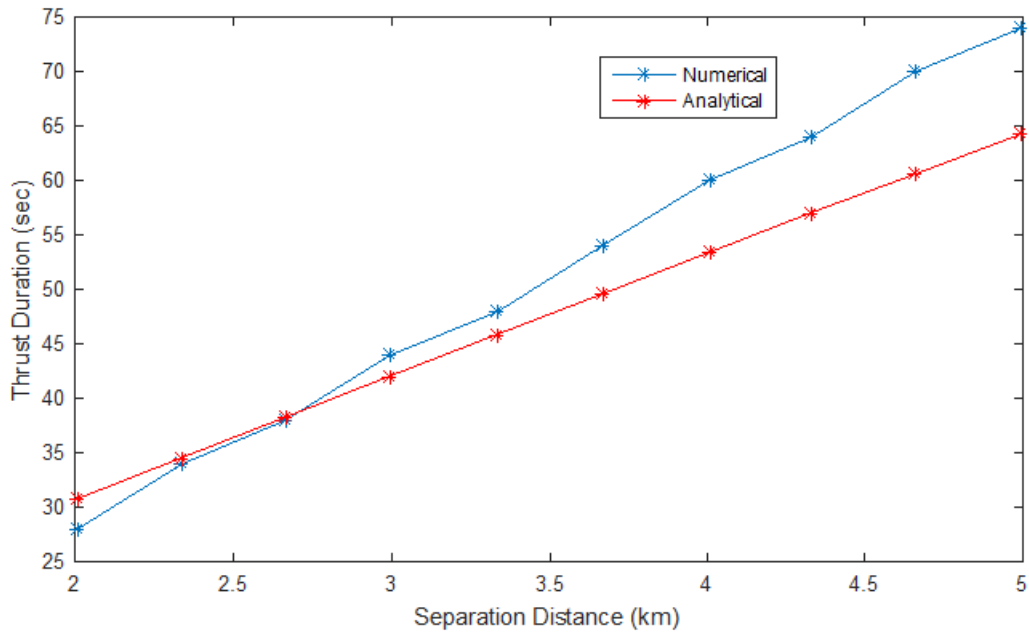


**Figure 8.1. Thrust Duration vs Separation Distance, Numerical and Analytical**

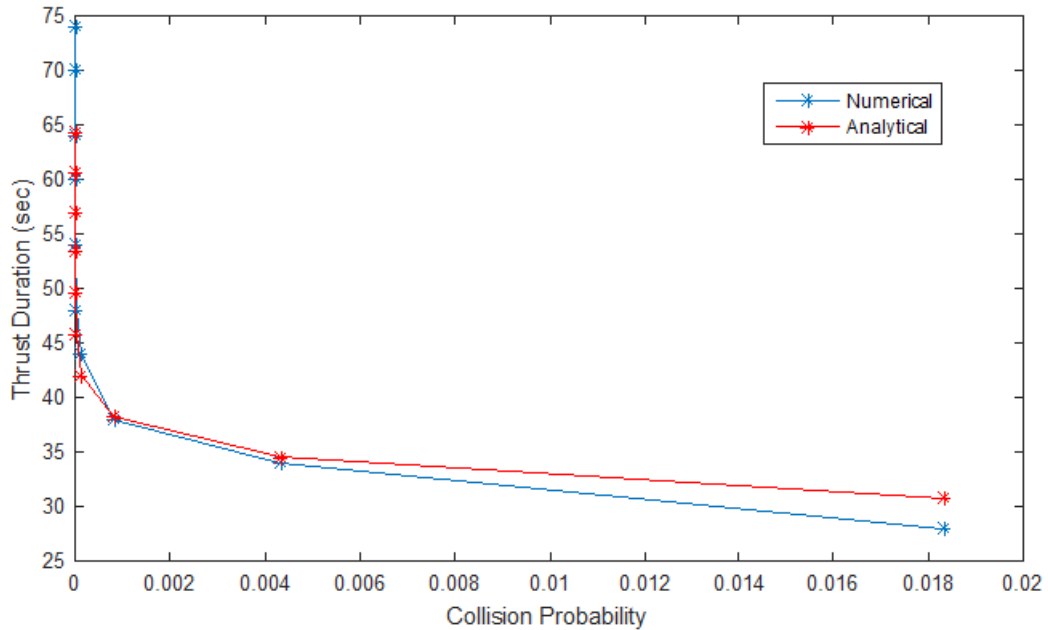


**Figure 8.2. Thrust Duration vs Collision Probability, Numerical and Analytical**

## 8.2 Trade Study Comparisons

In solving for the avoidance maneuver, the optimum burn duration was determined for various ranges of separation distance and maximum collision probability values. When determining, operationally, the desired collision probability, there is rarely a “correct answer.” This is where trade studies become useful. The spacecraft operators can choose weights for the three metrics (maximum collision probability, total maneuver duration, and total required  $\Delta V$ ) which allows them to narrow down the possible maneuver choices, if they elect to perform one at all.

For a 2000 kg, 180 N spacecraft in a circular 700 km orbit inclined to  $50^\circ$ , notification times of 8 minutes, 15 minutes, 20 minutes, and 30 minutes were considered and used for the trade studies. In addition, the covariance data is assumed to be equivalent to that used in Section 8.1. For all scenarios, the total  $\Delta V$  available for the

maneuver is assumed to be limited to less than 1 km/s in order to realistically trade the possible options. Increasing or decreasing this limitation would have a negligible effect on the results of this study.

When considering only an 8-minute notification time, this limitation on the total  $\Delta V$  significantly decreases our available maneuver options. Table 8.1 below shows the total required  $\Delta V$  and maneuver time for the minimum fuel and minimum time cases for each separation distance/collision probability value. The values in red denote those that exceed the 1 km/s limitation and those highlighted denote the options being traded. In this case, the minimum fuel case at a 0.1 km separation distance is being compared to the minimum fuel case at a 0.4 km separation distance.

**Table 8.1 Maneuver Options for 8-Minute Notification Time**

Separation Distance (km)	Probability	Min Fuel		Min Time	
		$\Delta V$ (km/s)	Time (min)	$\Delta V$ (km/s)	Time (min)
0.1	4.00E-12	0.120	106.8	66.57	39.67
0.2	3.99E-12	0.551	106.8	66.92	39.67
0.3	3.98E-12	0.733	106.2	67.10	39.67
0.4	3.97E-12	0.917	97.50	67.27	39.67
0.5	3.96E-12	1.101	91.83	69.42	39.67
0.6	3.94E-12	1.285	85.83	69.59	39.67
0.7	3.92E-12	1.470	79.83	69.77	39.67
0.8	3.90E-12	1.654	78.83	69.95	39.67
0.9	3.87E-12	1.840	73.50	70.12	39.67

To begin the trade study, since avoiding the collision is the main priority, the collision probability metric is given a weighting of 0.5 out of the total available 1.0. It is useful to note that the actual magnitude of the collision probability is not significant since the default covariance values used to find the maximum collision probability from the



desired separation distance is just assumed to be generic values. The significance is how the probability varies with the separation distance and required burn duration, which is unaffected by the relative magnitudes. The weights for the fuel use and maneuver time metrics are then both set to 0.25 to begin with (see Table 8.2). Because all  $\Delta V$  values for the minimum time cases exceed 1 km/s, no minimum time option is included in the trade. Instead, only the two minimum fuel options, one at the minimum collision probability, are compared. Because the minimum probability case also takes the least amount of time, the minimum probability case easily out-scores the minimum fuel case, and is highlighted in the trade study matrix.

**Table 8.2 Minimum Fuel Trade Studies for 8-Minute Notification Time, Equal Fuel and Time Weights**

		<b>Options</b>	
<b>Criteria</b>	<b>Weight</b>	Min Fuel	Min Probability
Probability	0.5	1	5
Fuel	0.25	5	1
Time	0.25	1	5
<b>Total</b>		2	4

The question now is what possible weighting schemes would make the minimum fuel solution more preferable. It was found that even weighing the fuel use at 4 times more significant than the maneuver time still does not overcome the 100% difference between the two total metric values. Table 8.3 shows that this trade still results in the minimum probability case dominating.

**Table 8.3 Minimum Fuel Trade Studies for 8-Minute Notification Time, Unequal Fuel and Time Weights**

Criteria	Weight	Options	
		Min Fuel	Min Probability
Probability	0.5	1	5
Fuel	0.4	5	1
Time	0.1	1	5
<b>Total</b>		2.6	3.4

It was found, actually, that only by decreasing the collision probability weight to 0.25 and increasing the fuel use weight to 0.5 do the two options become equivalent (seen in Table 8.4). This means that, for notification times around 8 minutes, choosing a maneuver that minimizes the collision probability would be the most logical choice unless there is a significant constraint on the fuel available for the maneuver.

**Table 8.4 Minimum Fuel Trade Studies for 8-Minute Notification Time, Unequal Fuel and Time Weights, Decreased Probability Weight**

Criteria	Weight	Options	
		Min Fuel	Min Probability
Probability	0.25	1	5
Fuel	0.5	5	1
Time	0.25	1	5
<b>Total</b>		3	3

Next, the same process can be repeated for a notification time of 15 minutes. As seen in Table 8.5, nearly doubling the notification time decreases the total  $\Delta V$  required for the minimum time cases, but not enough to fall beneath the 1 km/s limit. The available probability range widens for the minimum fuel case, however, for nearly the

same fuel cost as the 8-minute notification scenario. The notable change between the two is the separation distance values of the minimum fuel cases. When increasing the notification time to 15 minutes, the lowest separation distance no longer requires the least amount of fuel. Instead, a 0.2 km separation distance now minimizes the total  $\Delta V$ . This leads to a slight, but insignificant change in the trade studies compared to the 8-minute notification scenario. Once again, setting the probability weighting to 0.25, the fuel use weighting to 0.5, and the maneuver time weighting to 0.25 leads to the minimum fuel scenario only slightly beating out the minimum probability scenario. For both 8- and 15-minute notification times, choosing a maneuver that minimizes the collision probability would be the most logical choice unless there is a significant constraint on the fuel available for the maneuver.

**Table 8.5 Maneuver Options for 15-Minute Notification Time**

Separation Distance (km)	Probability	Min Fuel		Min Time	
		$\Delta V$ (km/s)	Time (min)	$\Delta V$ (km/s)	Time (min)
0.1	4.00E-12	0.203	128.8	13.20	46.50
0.2	3.99E-12	0.120	128.8	13.18	46.50
0.3	3.98E-12	0.374	128.8	13.33	46.50
0.4	3.97E-12	0.373	128.8	13.31	46.50
0.5	3.96E-12	0.557	128.8	13.46	46.50
0.6	3.94E-12	0.558	128.8	13.44	46.50
0.7	3.92E-12	0.743	128.8	13.59	46.50
0.8	3.90E-12	0.746	128.8	13.57	46.50
0.9	3.87E-12	0.931	127.17	13.73	46.50
1	3.84E-12	0.934	122.83	13.70	46.50

Increasing the notification time just an additional 5 minutes changes the scenario rather significantly. Table 8.6 shows the same separation distance ranges as the 15-minute notification case, but the additional available time decreases the required  $\Delta V$  so

much so that the minimum time solution now falls beneath the 1 km/s limit. As noted in the 15-minute notification scenario, the minimum separation distance value no longer results in the lowest  $\Delta V$ , and that holds true in this scenario as well. This time, the minimum  $\Delta V$  occurs at a separation distance of 0.3 km. It can also be noticed that the maneuver time between each minimum fuel and each minimum time case does not vary at these separation distances. Therefore, only the minimum fuel and minimum time options were chosen to be explored for the following trade study.

**Table 8.6 Maneuver Options for 20-Minute Notification Time**

		Min Fuel		Min Time	
Separation Distance (km)	Probability	$\Delta V$ (km/s)	Time (min)	$\Delta V$ (km/s)	Time (min)
0.1	4.00E-12	0.208	118.8	0.347	50.83
0.2	3.99E-12	0.203	118.8	0.339	50.83
0.3	3.98E-12	0.199	118.8	0.330	50.83
0.4	3.97E-12	0.376	118.8	0.502	50.83
0.5	3.96E-12	0.377	118.8	0.495	50.83
0.6	3.94E-12	0.378	118.8	0.487	50.83
0.7	3.92E-12	0.564	118.8	0.664	50.83
0.8	3.90E-12	0.566	118.8	0.660	50.83
0.9	3.87E-12	0.569	118.8	0.656	50.83
1	3.84E-12	0.757	118.8	0.840	50.83

Starting with the same initial weighting system (0.5 for probability, 0.25 for fuel use, and 0.25 for maneuver time), an identical trade study (Table 8.7) to that found in Table 8.2 was performed, except this occasion with the minimum time case instead of the minimum probability case. This time, with both cases having a higher collision probability and the fuel required for the minimum time case being only slightly higher than the minimum fuel case, the minimum time case results in the highest overall metric. This was found to hold true for all scenarios except when the fuel minimization metric is

chosen to be at least four times greater than the time minimization metric (Table 8.8). From this, it appears that at notification times of around 20 minutes and greater, the minimum time case becomes more ideal as the required total  $\Delta V$  for the maneuver is not significantly greater than that of the minimum fuel case.

**Table 8.7 Minimum Fuel, Minimum Time Trade Studies for 20-Minute Notification Time, Equal Fuel and Time Weights**

Criteria	Weight	Options	
		Min Fuel	Min Time
Probability	0.5	1.35	1.00
Fuel	0.25	5.00	4.08
Time	0.25	1.00	5.00
<b>Total</b>		2.18	<b>2.77</b>

**Table 8.8 Minimum Fuel, Minimum Time Trade Studies for 20-Minute Notification Time, Unequal Fuel and Time Weights**

Criteria	Weight	Options	
		Min Fuel	Min Time
Probability	0.5	1.35	1
Fuel	0.4	5	4.08
Time	0.1	1	5
<b>Total</b>		<b>2.78</b>	2.63

The difference between the total  $\Delta V$  required for the minimum fuel and minimum time cases becomes even smaller for a 30-minute notification time scenario. Just as was noted in the previous scenarios, the maximum separation distance achievable increased between the two cases, as did the separation distance value corresponding to the lowest  $\Delta V$  possible to complete the maneuver. In this trade study, in addition to the same

minimum fuel and minimum time cases, an additional minimum time case was chosen such that the maneuver time is equivalent, the separation distance is near the maximum achievable, and the  $\Delta V$  required is equivalent to that of the minimum fuel transfer for the same separation distance value.

**Table 8.9 Maneuver Options for 30-Minute Notification Time**

Separation Distance (km)	Probability	Min Fuel		Min Time	
		$\Delta V$ (km/s)	Time (min)	$\Delta V$ (km/s)	Time (min)
0.1	4.00E-12	0.228	128.8	0.237	58.17
0.2	3.99E-12	0.220	128.8	0.234	58.17
0.3	3.98E-12	0.212	128.8	0.230	58.17
0.4	3.97E-12	0.206	128.8	0.227	58.17
0.5	3.96E-12	0.201	128.8	0.224	58.17
0.6	3.94E-12	0.390	128.8	0.402	58.17
0.7	3.92E-12	0.392	128.8	0.399	58.17
0.8	3.90E-12	0.394	128.8	0.397	58.17
0.9	3.87E-12	0.395	67.83	0.395	58.17
1	3.84E-12	0.393	67.83	0.393	58.17
2	3.41E-12	0.768	67.83	0.768	58.00

Like in the previous trade studies, the same initial weighting system (0.5 for probability, 0.25 for fuel use, and 0.25 for maneuver time) was chosen. The three cases can be seen compared in Table 8.10. As the minimum probability case out performs the other cases in the collision probability metric, has an equivalent timing metric value to the minimum time case, and does not perform poorly in fuel consumption despite having the highest  $\Delta V$  of the three cases, it just barely wins out over the minimum time case. Only when the fuel weighting is increased to four times the time weighting do the results change (Table 8.11). Despite the emphasis placed on minimizing the fuel usage, the minimum time case now stands out because, despite the slight increase in the required  $\Delta V$ , it significantly out performs the minimum fuel case with regards to the maneuver

time. It was found that only when increasing the fuel metric weighting to nearly 0.9 does the minimum fuel case dominate over the minimum time case.

**Table 8.10 Minimum Fuel, Minimum Time, Min Probability Trade Studies for 30-Minute Notification Time, Equal Fuel and Time Weights**

		<b>Options</b>		
<b>Criteria</b>	<b>Weight</b>	Min Fuel	Min Time	Min Probability
Probability	0.5	1.27	1	1.87
Fuel	0.25	5	4.75	3.64
Time	0.25	1	4.99	4.99
<b>Total</b>		2.14	2.93	<b>3.09</b>

**Table 8.11 Minimum Fuel, Minimum Time, Min Probability Trade Studies for 30-Minute Notification Time, Unequal Fuel and Time Weights**

		<b>Options</b>		
<b>Criteria</b>	<b>Weight</b>	Min Fuel	Min Time	Min Probability
Probability	0.5	1.27	1	1.87
Fuel	0.4	5	4.75	3.64
Time	0.1	1	4.99	4.99
<b>Total</b>		2.74	<b>2.90</b>	2.89

When comparing all four trade studies side-by-side, a few conclusions can be made for use in future satellite mission design and operations. First, and most notable, is that choosing to avoid the collision at a higher probability threshold does not always guarantee the lowest required fuel use or time for the maneuver. The higher the notification time, the more the required fuel can be minimized by choosing a lower collision probability threshold. In addition, for collision avoidance maneuvers with notification times less than about 20 minutes, the most logical choice would be the

maneuver that minimizes the collision probability unless significant emphasis is placed on fuel savings. For collision avoidance maneuvers with notification times greater than 20 minutes and less than one orbital period, the minimum time solution becomes the most logical option while also minimizing the collision probability as much as the onboard fuel supply will allow. Fortunately, as the notification time increases, the required  $\Delta V$  values increase less with decreasing collision probability thresholds. This means that, with only basic constraints on the fuel available for the maneuver, it is still possible to minimize both the collision probability threshold and total maneuver time with the preferred solution. These observations would allow for an optimal collision probability threshold to be chosen in future missions given the weights of each metric and the available fuel at the time of the maneuver.



## **Chapter 9**

### **Conclusions**

Currently, on-orbit assets are susceptible to unpredicted debris-creating events. As discussed, satellite collision avoidance maneuvers for such events become more complex (such as the necessity for finite burn analysis) since the time-to-collision is minimal. This short amount of time available to both plan and execute the maneuver means that the speed at which the burn time for the maneuver can be determined is significant. In the case that such a scenario is encountered, a technique was devised in order to find a semi-analytical solution that could be calculated at a moment's notice given only the parameters of the spacecraft and the location of the collision. This resulted in a solution for the majority of the necessary quick response collision avoidance maneuvers in Low-Earth Orbit, assuming only that the covariance of the debris cloud is oriented along its velocity vector. Such an analytical solution could be provided as onboard software for both current and future satellites and would result in nearly-autonomous collision avoidance when it is needed the most.

In many cases, it is desirable to optimize the whole maneuver to include the return trajectory as well in order to ensure that decreasing the collision probability is worth the effect of the maneuver on the mission operations. Whether limitations are placed on the maneuver by the amount of fuel available onboard or restrictions on the orbital position of the spacecraft, all three metrics must be considered through the use of a trade study to

determine the best course of action. While, in some cases, the best action may be not to move the spacecraft at all, the assumption was made that a maneuver was necessary when performing the trade studies. It was found that, for notification times less than around 20 minutes, it is best to decrease the collision probability as much as the available fuel will allow. As the notification time increases past 20 minutes, more emphasis can be placed on the time required to perform the entire maneuver and it was found that simultaneously minimizing the maneuver time and collision probability outweighed the slight extra fuel required for such a maneuver. While the mission requirements and satellite characteristics will vary widely between collision scenarios, this information can be considered by mission designers when allocating onboard fuel for such maneuvers and by satellite operators when determining the best course of action to avoid an impending collision. In rapid collision avoidance maneuvers, not much time can be spent determining the optimal collision probability threshold. With this work, just by knowing the desired weighting for the metrics and basic covariance data, an optimal collision probability threshold can be chosen for the maneuver and used to calculate the necessary burn duration from the generated analytical equation.

## REFERENCES

1. F. K. Chan, *Spacecraft Collision Probability*. The Aerospace Press, American Institute of Aeronautics and Astronautics, Inc., 2008.
2. Ailor, W.H., and G.E. Peterson, "Collision Avoidance As A Debris Mitigation Measure," IAC-04-IAA.5.12.3.01, *55th International Astronautical Congress*, Vancouver, Canada, October 4-8, 2004.
3. E. Frazzoli, E. Dahleh, M. A. Feron, and R. P. Kornfeld, "A Randomized Attitude Slew Planning Algorithm For Autonomous Spacecraft," AIAA 2001-4155, *AIAA Guidance, Navigation, and Control Conference and Exhibit*, 2001.
4. Kessler, D. J., "Sources of Orbital Debris and the Projected Environment for Future Spacecraft," *Journal of Spacecraft and Rockets*, Vol. 18, No. 4, July-Aug. 1981, pp. 357-360.
5. Russell P. Patera and Glenn E. Peterson. "Space Vehicle Maneuver Method to Lower Collision Risk to an Acceptable Level," *Journal of Guidance, Control, and Dynamics*, Vol. 26, No. 2 (2003), pp. 233-237.
6. Alfano S, "Collision Avoidance Maneuver Planning Tool," AAS 05-308, *15th AAS/AIAA Astrodynamics Specialist Conference*, Lake Tahoe, CA, 7-11 Aug 2005.
7. E. Kim, H. Kim, H. Kim, "Optimal Solution of Collision Avoidance Maneuver with Multiple Space Debris," *Journal of Space Operations*, Vol. 9, No. 3 (2012).

8. C. Bombardelli, "Analytical Formulation of Impulsive Collision Avoidance Dynamics," *Celestial Mechanics and Dynamical Astronomy*, 2013.
9. C. Bombardelli, J.H. Ayuso, R.G. Pelayo, "Collision Avoidance Maneuver Optimization," AAS 14-355, *24<sup>th</sup> Space Flight Mechanics Meeting*, Sante Fe, NM, Jan 2014.
10. K. Lee, C. Park., S. Park., "Near-Optimal Guidance and Control for Spacecraft Collision Avoidance Maneuvers," AIAA 2014-4114, *15th AAS/AIAA Astrodynamics Specialist Conference*, Lake Tahoe, CA, 7-11 Aug 2005.
11. Scharf, D. P., Acikmese, B., Ploen, S. R., and Hadaegh, F. Y. "Three-Dimensional Reactive Collision Avoidance with Multiple Colliding Spacecraft for Deep-Space and Earth-Orbiting Formations," *4th International Conference on Spacecraft Formation Flying Missions & Technologies*, St-Hubert, Quebec 2011.
12. Prussing, John E., and Bruce A. Conway. *Orbital Mechanics*. New York: Oxford UK, 1993.
13. Curtis, Howard D. (2013). *Orbital Mechanics for Engineering Students* (3rd ed.). Butterworth-Heinemann.
14. Chobotov, Vladimir A. *Orbital Mechanics*. Washington, DC: American Institute of Aeronautics and Astronautics, 1991.
15. R.H. Battin. *Introduction to the Mathematical Methods of Astrodynamics*. AIAA Education series, 1987, New York.
16. Kaula, William M. *Theory of Satellite Geodesy: Applications of Satellites to Geodesy*. Waltham, Mass.: Blaisdell Pub. Co., 1966.

17. Vallado, David A. *Fundamentals of Astrodynamics and Applications*. 3rd ed.  
Dordrecht: Kluwer Academic, 2007.
18. Wertz, James R, David F. Everett, and Jeffery J. Puschell. *Space Mission Engineering: The New SMAD*. Hawthorne, CA: Microcosm Press, 2011.
19. Montgomery, Douglas C, Elizabeth A. Peck, and G G. Vining. *Introduction to Linear Regression Analysis*. New York: Wiley, 2001.